Export of anthropogenic reactive nitrogen and sulfur compounds from the East Asia region in spring

M. Koike,[1] Y. Kondo,[2] K. Kita,[3] N. Takegawa,[2] Y. Masui,[1] Y. Miyazaki,[2] M. W. Ko,[4] A. J. Weinheimer,[5] F. Flocke,[5] R. J. Weber,[6] D. C. Thornton,[7] G. W. Sachse,[4] S. A. Vay,[4] D. R. Blake,[8] D. G. Streets,[9] F. L. Eisele,[5] S. T. Sandholm,[6] H. B. Singh,[10] and R. W. Talbot[11]

Received 4 December 2002; revised 17 April 2003; accepted 2 May 2003; published 31 October 2003.

[1] Measurements of gaseous and particulate reactive nitrogen and sulfur species, as well as other chemical species, were made using the P-3B and DC-8 aircraft over the western Pacific during the NASA Transport and Chemical Evolution over the Pacific (TRACE-P) experiment, conducted between February and April 2001. These measurements provide a good opportunity to study the extent to which anthropogenic NO_x and SO_2 emitted over the East Asian countries remain as NO_y and SO_x ($=SO_2 + nssSO_4^{2-}$) in the form of gas or fine particles when an air mass is transported into the western Pacific region. In this paper a method to estimate transport efficiencies, $\varepsilon(NO_y)$ and $\varepsilon(SO_x)$, in an air mass that has experienced multiple injection, mixing, and loss processes is described. In this analysis, CO and CO_2 are used as passive tracers of transport, and the emission inventories of CO, CO_2, NO_x, and SO_2 over the East Asia region are used. Results from the P-3B presented in this study indicate that 20–40% and 15% of NO_x emitted over the northeastern part of China remained as NO_y over the western Pacific in the boundary layer (BL) and free troposphere (FT), respectively. In the FT, PAN is found to have been the dominant form of NO_y, while only 0.5% of emitted NO_x remained as NO_x. The transport efficiency of SO_x is estimated to have been 25–45% and 15–20% in the BL and FT, respectively. Median values of the $nssSO_4^{2-}/SO_x$ ratio are 0.4–0.6 both in the BL and FT, however large variability is found in the FT. These results are generally consistent with those derived using DC-8 data. The results obtained in this study indicate that more than half of NO_y and SO_x were lost over the continent and that the vertical transport from the BL to FT further reduced their amounts by a factor of 2, likely due to wet removal. Budgets of NO_y and SO_x were also studied for air masses, which we sampled during TRACE-P and the flux out from the continent in these cases is estimated to be 20% of the emissions. Flux in the BL and FT is found to have a similar contribution. *INDEX TERMS:* 0305 Atmospheric Composition and Structure: Aerosols and particles (0345, 4801); 0345 Atmospheric Composition and Structure: Pollution—urban and regional (0305); 0368 Atmospheric Composition and Structure: Troposphere—constituent transport and chemistry; 0365 Atmospheric Composition and Structure: Troposphere—composition and chemistry; *KEYWORDS:* reactive nitrogen, nitrate, sulfur dioxide, sulfate, transport, East Asia

Citation: Koike, M., et al., Export of anthropogenic reactive nitrogen and sulfur compounds from the East Asia region in spring, *J. Geophys. Res.*, *108*(D20), 8789, doi:10.1029/2002JD003284, 2003.

1. Introduction

[2] Anthropogenic emissions of nitrogen oxides (NO_x = NO + NO_2) and sulfur dioxide (SO_2) in East Asian countries are of great concern because of their impact on the atmospheric environment on regional and intercontinental scales. These two compounds play critical roles in controlling the oxidizing power of the atmosphere (primarily by NO_x) and air quality, causing acid rain, and changing radiative forcing, through gas-phase chemistry and particle formation. Rapid economic growth and increasing fossil fuel energy consumption in the People's Republic of China in the past 2 decades has resulted in large emissions of reactive nitrogen and sulfur compounds into the atmosphere. China is expected to undergo further economic

[1]Department of Earth and Planetary Science, Graduate School of Science, University of Tokyo, Tokyo, Japan.
[2]Research Center for Advanced Science and Technology, University of Tokyo, Tokyo, Japan.
[3]Department of Environmental Science, Graduate School of Science, Ibaraki University, Ibaraki, Japan.
[4]NASA Langley Research Center, Hampton, Virginia, USA.
[5]National Center for Atmospheric Research, Boulder, Colorado, USA.
[6]Georgia Institute of Technology, Atlanta, Georgia, USA.
[7]Drexel University, Philadelphia, Pennsylvania, USA.
[8]University of California, Irvine, Irvine, California, USA.
[9]Argonne National Laboratory, Argonne, Illinois, USA.
[10]NASA Ames Research Center, Moffett Field, California, USA.
[11]University of New Hampshire, Durham, New Hampshire, USA.

0148-0227/03/2002JD003284$09.00

Table 1. Measurements Onboard the NASA P-3B and DC-8 Aircraft During TRACE-P

Species	Aircraft	Technique	Reference
CO	P-3B, DC-8	Differential absorption technique using a tunable diode laser	*Sachse et al.* [1987]
CO_2	P-3B, DC-8	Nondispersive infrared (NDIR) analyzers	*Vay et al.* [1999]
NO, NO_2, NO_y	P-3B	Chemiluminescence/photolysis converter/gold catalytic converter	*Kondo et al.* [1997]
NO, NO_2	DC-8	Two-photon laser-induced fluorescence (TP-LIF)	*Bradshaw et al.* [1999]
PAN	P-3B	GC/ECD	
PAN	DC-8	GC/ECD	*Singh et al.* [1996]
HNO_3	P-3B	CIMS	*Mauldin et al.* [1998]
HNO_3	DC-8	Mist chamber/ion chromatography	*Talbot et al.* [1997]
SO_2	P-3B	Atmospheric pressure ionization mass spectrometry (APIMS)	*Thornton et al.* [2002]
SO_2	DC-8	Mist chamber/ion chromatography	
SO_4^{2-} and NO_3^-	P-3B	Particle-into-liquid sampler (PILS)	*Weber et al.* [2001]
SO_4^{2-}	DC-8	Mist chamber/ion chromatography	*Scheuer et al.* [2002]
NMHCs/halocarbons	P-3B, DC-8	Whole air samples/GC/FID/ECD/MS	*Blake et al.* [2001]

growth and modernization in the next several decades. Emissions of SO_2 from China, however, are estimated to have reached a peak level in 1996, followed by a slow decline, due to a combination of environment regulations and other factors, although the primary energy source still relies on coal burning [*Streets et al.*, 2000; *Streets et al.*, 2003]. Emissions of NO_x due to commercial energy use in China are also estimated to have been the greatest in 1996, with a subsequent declining trend, mainly due to the reduction of coal consumption [*Hao et al.*, 2002]. Consequently, future emissions of NO_x and SO_2 from China will be less than those anticipated in the early to mid-1990s. Nevertheless, current emissions from China are still large and dominant in Asia for NO_x (42%) and SO_2 (59%) [*Streets et al.*, 2003], and a further increase in NO_x emissions is anticipated in Southeast Asia and the Indian subcontinent [*van Aardenne et al.*, 1999].

[3] Anthropogenic emissions of NO_x and SO_2 occur predominantly at the continental surface, and chemical conversion and loss processes take place within the boundary layer. Eventually, these air masses leave the source region via horizontal transport within the boundary layer and free troposphere. The concentrations in the free troposphere are usually smaller than in the boundary layer because a large fraction of the species is removed in the boundary layer before transported to the free troposphere. Wet deposition of soluble species during vertical transport further reduces the influences from anthropogenic emissions. On the other hand, long-range horizontal transport in the free troposphere is more efficient due to an increasing westerly wind speed with altitude. Thus it is not immediately obvious whether transport through the boundary layer or free troposphere is more efficient in bringing emitted material to the western Pacific. Processes of transport and the regional budget of anthropogenic reactive nitrogen and sulfur compounds over the East Asia region have been studied by many investigators using three-dimensional model simulations [e.g., *Bey et al.*, 2001; *Xiao et al.*, 1997; *Chin et al.*, 2000; *Tan et al.*, 2002]. In these studies, observations such as aircraft measurements made during the Pacific Exploratory Mission in the Western Pacific Ocean (PEM-West) were used to evaluate the validity of the model calculations. However, measurements which can be used for quantitative evaluation are still limited.

[4] Measurements of gaseous and particulate compounds of reactive nitrogen and sulfur species, as well as other chemical species, were made from the NASA P-3B and DC-8 aircraft over the western Pacific during the NASA Transport and Chemical Evolution over the Pacific (TRACE-P) experiment, conducted between February and April 2001 [*Jacob et al.*, 2003]. The major goal of the TRACE-P experiment is to evaluate the impact of outflow from Asia, especially that of anthropogenic emissions over the Asian continent, on the atmospheric environment.

[5] During the TRACE-P experiment, air masses that had been influenced by anthropogenic emissions over China and other East Asian countries, were occasionally encountered. Using these data, we estimate the extent to which anthropogenic reactive nitrogen and sulfur compounds emitted over the northeastern part of China were transported into the western Pacific region (in the form of gas + fine particles). The method uses measured concentrations of CO and CO_2 as indicators for an amount of material injected into the sampled air mass. The background levels of CO, NO_y, and SO_x (= SO_2 + $nssSO_4^{2-}$) are estimated for individual air masses, and the increases in their concentrations above the background levels, ΔCO, ΔNO_y, and ΔSO_x, are derived from the measurements. Ratios of increases, $\Delta NO_y/\Delta CO$ and $\Delta SO_x/\Delta CO$, are then compared with emission ratios E_{NOx}/E_{CO} and E_{SO2}/E_{CO}. We define a transport efficiency $\varepsilon(NO_y)$ and $\varepsilon(SO_x)$, as follows:

$$\varepsilon(NO_y) = \Delta NO_y/[\Delta CO \times E_{NOx}/E_{CO}] \quad (1)$$

$$\varepsilon(SO_x) = \Delta(SO_2 + nssSO_4^{2-})/[\Delta CO \times E_{SO2}/E_{CO}] \quad (2)$$

The denominators are the expected increase in NO_y or SO_x in the absence of removal processes deduced from the observed ΔCO value, while the numerators are the observed increases, ΔNO_y or ΔSO_x. In this paper, a method to estimate the transport efficiencies, $\varepsilon(NO_y)$ and $\varepsilon(SO_x)$, in an air mass that has experienced multiple injection, mixing, and loss processes, is described. Vertical profiles of $\varepsilon(NO_y)$ and $\varepsilon(SO_x)$ are presented and possible processes resulting these efficiencies are discussed. Most of the analyses are made using the P-3B data set because NO_y measurements are available. The DC-8 data set is used to compare the results from the two platforms to confirm the results from the P-3B.

2. Measurements

[6] In this study, gas and aerosol data obtained on board the NASA P-3B and DC-8 aircraft were used. Techniques used for these measurements are listed in Table 1, as well as their references.

[7] The treatment of aerosol measurements is briefly described here. In the measurements of NO_y onboard the P-3B, NO_y compounds were catalytically converted to NO on the surface of a heated gold tube with the addition of CO, and NO was subsequently detected by an NO-O_3 chemiluminescence technique [*Kondo et al.*, 1997; *Koike et al.*, 2002]. Although the inlet tube for air sampling faced rearward, particles with diameters smaller than about 1.5 and 1.1 μm are considered to have been sampled by the NO_y instrument at altitudes of 0.5 and 6 km, respectively (B. Liley, personal communication, 2003). Because of the operating temperature of the NO_y converter (300°C), ammonium nitrate (NH_4NO_3, boiling point 210°C) would be expected to thermally dissociate, while sodium nitrate ($NaNO_3$, boiling point 380°C) and calcium nitrate ($Ca(NO_3)_2$, melting point 561°C) would not be converted.

[8] Aerosol particle chemical composition, such as sulfate (SO_4^{2-}) and nitrate (NO_3^-), were measured onboard the P-3B, using a particle-into-liquid sampler (PILS) [*Weber et al.*, 2001]. The collection efficiency of particles with diameters smaller than 0.7 μm was estimated to be about 90%, decreasing to 50% for particles with diameters of 1.2 μm. The efficiency for particles larger than 3 μm in diameter was negligible [*Ma et al.*, 2003]. This collection efficiency was similar to that of the NO_y instrument, and both instruments are considered to sample particles in a similar size range, i.e., fine particles.

[9] Sulfate aerosol measurements onboard the DC-8 were made using a mist chamber and ion chromatography (MC-IC) technique. The median upper particle size cutoff was estimated to be 2.7 μm in diameter [*Scheuer et al.*, 2003]. Because of this larger cutoff size as compared with that of the PILS instrument, a greater number of coarse mode dust particles including calcium sulfate ($CaSO_4$), is expected to have been sampled. During the three P-3B/DC-8 intercomparison flights made during TRACE-P, agreements within 30–50% were found between P-3B/PILS and DC-8/MC-IC SO_4^{2-} measurements [*Ma et al.*, 2003]. The MC-IC values were systematically lower during one of the intercomparison flights in spite of larger cutoff size, suggesting that the observed differences were resulted from the error in the measurements.

[10] For the P-3B data set, amounts of non-sea-salt sulfate ($nssSO_4^{2-}$) were calculated from measurements of SO_4^{2-} and Na^+ using an empirical relationship in seawater. Because Na^+ data in the MC-IC SO_4^{2-} size range is not available for the DC-8 data set, SO_4^{2-} values are used as $nssSO_4^{2-}$ values. In this study, we denote SO_2 + $nssSO_4^{2-}$ as SO_x, which is considered to be a product of anthropogenic SO_2 emissions.

[11] For analyses using the P-3B data set, all data were averaged to the PILS aerosol-sampling time interval of about 3 min. For analyses using the DC-8 data set, all data were averaged for the mist chamber sampling time interval of about 1 min.

3. Study Area and Emission Data

3.1. Study Area

[12] Figure 1 shows the flight tracks of the P-3B aircraft during TRACE-P. Five-day kinematic back trajectories of air masses sampled from the P-3B were calculated using the method described by T. A. Yamanouchi et al. (Arctic

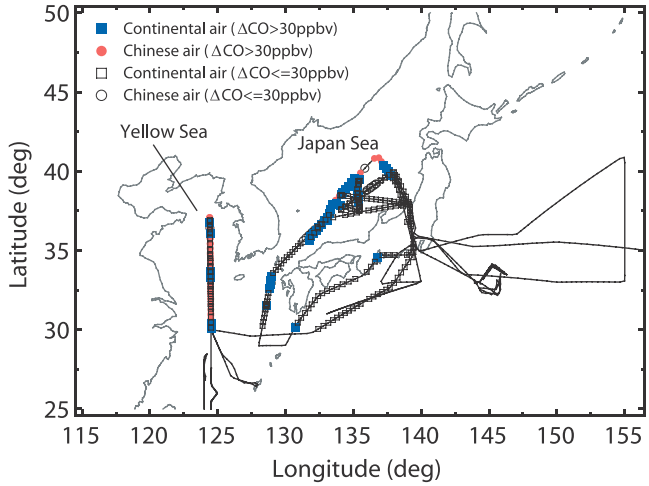

Figure 1. Flight tracks of the NASA/P-3B during TRACE-P. Locations where "continental air masses" and "Chinese air masses" were sampled are also shown. "Continental air masses" are those sampled in the study area defined as 30°N–42°N and 124°E–140°E (excluding air masses that could have been influenced by a volcano on Miyakejima Island). "Chinese air masses" are a subset of "continental air masses" and are those passed over China at altitudes below the 800-hPa level (boundary layer) within 5 days prior to measurement without passing over South Korea or Japan at these low altitudes. Locations where air masses in which ΔCO > 30 ppbv were sampled (signature of influences from anthropogenic emissions) are also shown.

Study of Tropospheric Aerosol and Radiation (ASTAR2000) campaign: An overview and first results, submitted to *Bulletin of the American Meteorological Society*, 2003), with meteorological data provided by the European Centre for Medium-Range Weather Forecasts (ECMWF) on a 1° × 1° latitude-longitude grid. For the present study, we defined the study area as 30°N–42°N and 124°E–140°E and trajectories for air masses sampled in this area are shown in Figure 2. A latitudinal boundary of 30°N was chosen because back trajectories of air masses sampled south of 30°N (17°N–30°N) passed over Southeast Asia, where hot spots due to biomass burning were frequently observed by the Advanced Very High Resolution Radiometer (AVHRR) satellite instrument during the TRACE-P period [*Heald et al.*, 2003]. In fact, air masses likely influenced by biomass burning (high CH_3Cl and K^+ concentrations) were occasionally observed at these latitudes in the free troposphere. A longitudinal boundary of 140°E was chosen, because a volcano on Miyakejima Island (34°N, 139°E) was quite active during the TRACE-P period, and a huge amount of SO_2 was likely emitted from it. Furthermore, air masses which could have been influenced by the Miyakejima Island volcano were discarded based on back trajectory analysis. As seen in Figure 2, almost all of the air masses sampled in the study area were transported from over the continent at latitudes between 30°N and 60°N by predominant westerly flow [*Fuelberg et al.*, 2003]. These air masses are expected to have been influenced by anthropogenic emissions over the continent, and we therefore denoted air masses sampled in the study area as "continental air masses." They were sampled during five flights (P-3B flight 13, 14, 16, 18, and 19) made between March 17 and April 2.

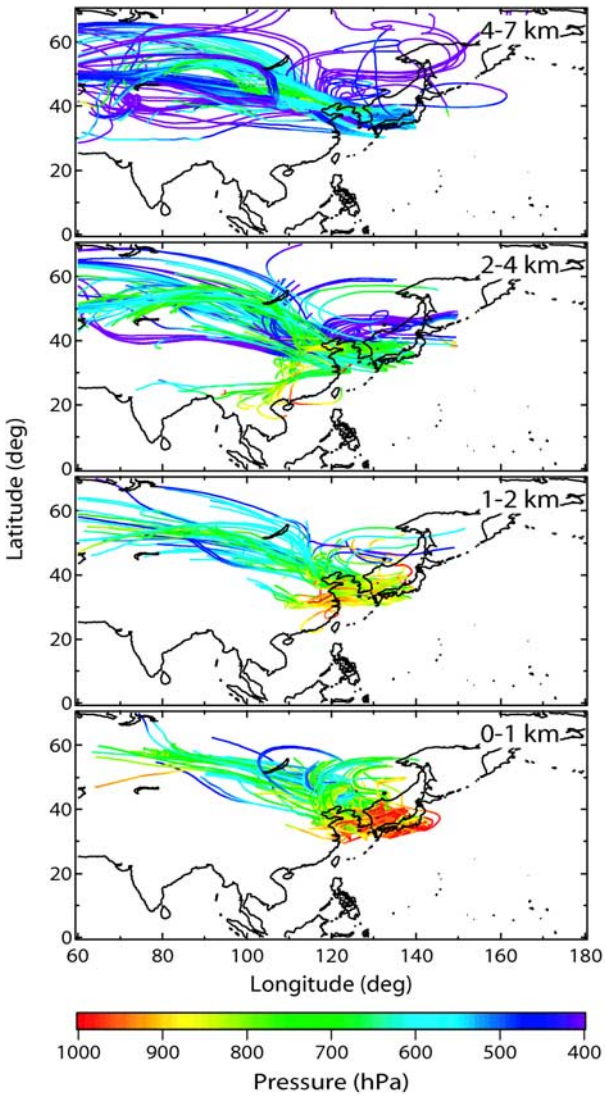

Figure 2. Five-day backward trajectories for air masses sampled by the P-3B aircraft in the study area (30°N–42°N and 124°E–140°E). Color of the trajectories shows atmospheric pressure along the trajectories.

[13] Emission ratios of CO, CO_2, NO_x, and SO_x (described in the next section) in Japan and the Republic of Korea (South Korea) are different from those in China. We thus further distinguished "Chinese air masses" from "continental air masses" using back trajectories. "Chinese air masses" are defined as those that passed over China at altitudes below the 800-hPa level (boundary layer) within 5 days prior to the measurements. We excluded air masses of Chinese origin that passed over South Korea and/or Japan at altitudes below 800 hPa. Locations where "Chinese air masses" were sampled are shown in Figure 1. They are a subgroup of "continental air masses" and will be used to confirm the results of the influences from China derived using "continental air masses."

3.2. Emission Data

[14] A comprehensive inventory of air pollutant emissions in Asia was developed for the year 2000 [*Streets et al.*, 2003]. For this estimate, all major contributing sources, such as power plants (coal and oil), transportation (oil), industrial sources (coal and oil), domestic sources (coal and biofuel), and biomass burning were taken into account. Because emissions of various species were calculated from the common model of activity rate (e.g., fossil fuel energy use rate), these estimates are considered to be internally consistent. In general, other emission estimates were made in less consistent ways, as different investigators use different models for different species. The consistency of emission estimates is important in the present study, because we estimated the transport efficiency using emission ratio information, as shown in equations (1) and (2).

[15] In this study, emission data for CO, CO_2, NO_x, and SO_2 were used. Figure 3 shows the emissions of these species in the East Asian countries in the year 2000. High-emission regions are generally located in the coastal area of the northeastern part of China, South Korea, and Japan. Annual emissions from China were estimated to be 4.13 tera-mol (Tmol) for CO, 86.7 Tmol for CO_2, 0.247 Tmol for NO_x, and 0.318 Tmol for SO_2 with a 95% confidence level of ±156%, ±16%, ±23%, and ±13%, respectively [*Streets et al.*, 2003]. Uncertainty is greatest for CO because emission factors are highly dependent on the efficiency of the combustion process. In fact, a comparison of model calculations using this emission inventory with observations suggests that CO estimates for China are low [*Palmer et al.*, 2003; *Carmichael et al.*, 2003]. It is noted that although annual average emission rates are used in this study, emissions in March (TRACE-P period) are close to the annual averages [*Streets et al.*, 2003].

[16] In Figures 4a–4c the correlation between the emission rates of CO, CO_2, NO_x, and SO_2 in the northeastern part of China within the region of 25°N–50°N and 100°E–130°E (except for South Korea) is shown using gridded emission data with a spatial resolution of 1° × 1°. This region was chosen because most of the air masses sampled in the study area (30°N–42°N and 124°E–140°E) were transported through this region. As seen in these figures, emission rates assigned to each grid point show positive correlations with CO emissions. A correlation coefficient is slightly better when CO_2 is used instead of using CO as a reference gas; r^2 value for NO_x-CO_2 and SO_x-CO_2 is 0.96 and 0.82, respectively. These good correlations are unexpected because the emission ratios E_{CO}/E_{CO2}, E_{NOx}/E_{CO}, and E_{SO2}/E_{CO} in China are actually quite different for different emission sources. For example, coal-fired power plants are the largest source for SO_2 and NO_x in China, though CO emission from this source is negligible [*Streets et al.*, 2003]. It is likely that large sources of CO (such as transportation) are colocated with these power plants and a relatively good correlation has resulted. Our method to estimate the transport efficiency defined by equations (1) and (2) requires the same emission ratio be used for all air masses influenced by local emissions at different locations. Further refinements of the emission database should indicate whether the assumption can be justified.

[17] Total emissions in the region of 25°N–50°N and 100°E–130°E, except for emissions from South Korea, are given in Table 2. They correspond to about 70% of the total emissions from China. In Table 2, ratios of these total amounts are also given and are shown using solid lines in Figures 4a–4c. We used these values as E_{CO}/E_{CO2},

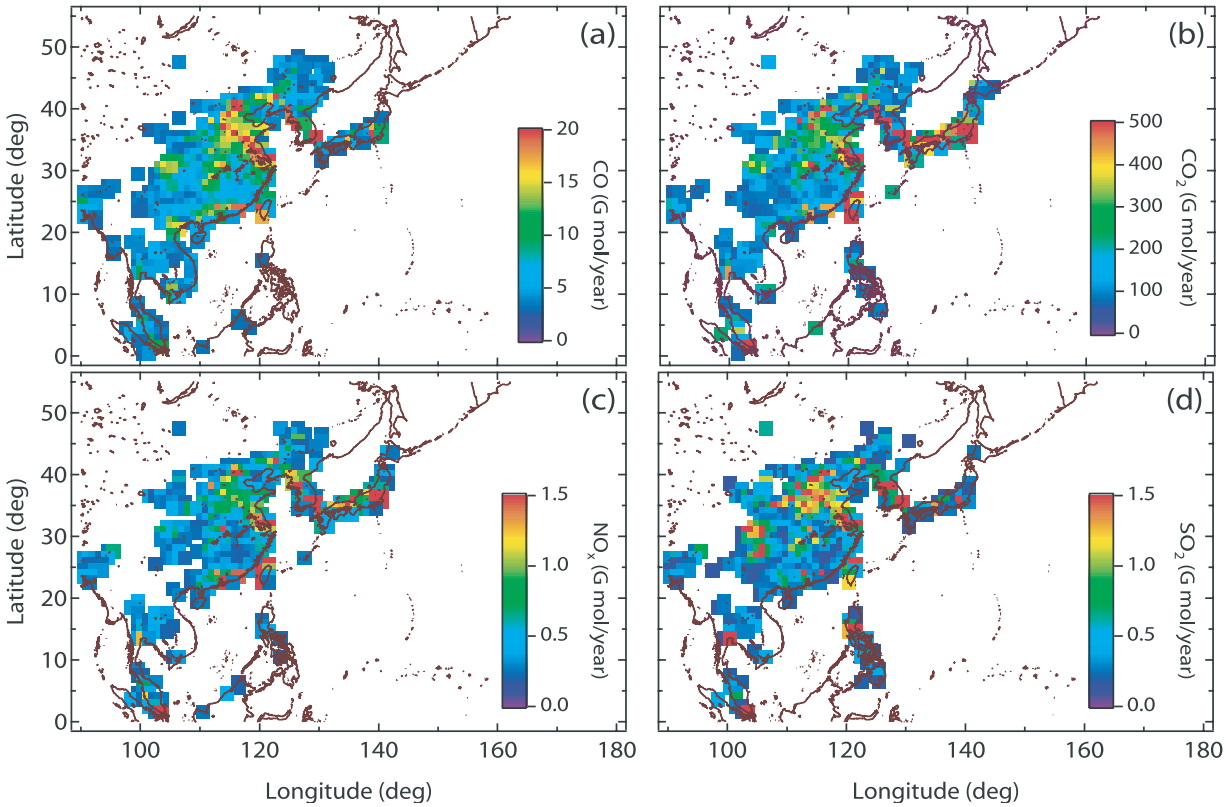

Figure 3. Distribution of anthropogenic emissions of (a) CO, (b) CO_2, (c) NO_x, and (d) SO_2 for the year 2000 at 1° × 1° resolution [*Streets et al.*, 2003]. To distinguish high-emission areas, only areas in which emissions are higher than certain criteria (CO > 3 Gmol/yr, CO_2 > 70 Gmol/yr, NO_x > 0.2 Gmol/yr, and SO_2 > 0.15 Gmol/yr) are plotted. Note that emissions greater than the highest values given in color-scales are also shown using the highest color-code (red).

E_{NOx}/E_{CO}, and E_{SO2}/E_{CO} ratios as representative of the emissions in the region in the following analyses. The values are not very sensitive to small change in the locations of the boundary because the boundary of the chosen region is far away from the locations of highest emissions.

[18] It is noted that emission ratios of CO, CO_2, NO_x, and SO_2 in South Korea and Japan are very different from those in China (Table 2): E_{NOx}/E_{CO} is larger, while E_{CO}/E_{CO2} is smaller. The value of E_{SO2}/E_{CO} in South Korea is also larger than that in China. Consequently, influences from South Korean and Japanese emissions are expected to be different from those from Chinese emissions that we estimate in this study. These influences are examined in the following sections and uncertainties in the transport efficiency estimates are discussed in section 5.7.

4. Approach

4.1. Estimation of Transport Efficiency

[19] As described in section 1, the transport efficiency of anthropogenically emitted reactive nitrogen and sulfur compounds, defined in equations (1) and (2), was estimated in the present study. For this purpose, background levels of CO, CO_2, NO_y, and SO_x were determined for individual sampled air masses, instead of using common values for all air masses. The definition of the "background value" of an air mass in this study is the value, which an air mass would have had if it had not been influenced by anthropogenic sources in the East Asian countries.

[20] To describe our approach to the transport efficiency estimation, an example of the CO-CO_2 relationship is shown in Figure 5a. An air mass can be identified as a point in the diagram by the measured CO and CO_2 concentrations. We made two simple assumptions in our analyses. First, CO and CO_2 values in background air masses have a linear relationship. Second, the emission ratio, E_{CO}/E_{CO2}, is constant so that the ratio of increases between CO and CO_2 ($\Delta CO/\Delta CO_2$) is always equal to the emission ratio when an air mass receives anthropogenic emissions. An argument for the validity of the first assumption is described in the next section. The second assumption is supported by the relatively good correlation between emissions of CO and CO_2 shown in Figure 4a. In addition, we assumed the loss of CO and CO_2 is negligible. Because air masses were sampled in our study area only 0 to 5 days after leaving the continent, this assumption is also reasonable.

[21] In Figure 5a, A and B are background air masses, and a line connecting them shows the background linear relationship. Let us assume an air mass C is produced by the mixing of A and B. Air mass C can also be considered as a background air mass, because it is not affected by anthropogenic emissions. Now let us assume another case in which both air masses A and B receive (different amounts of) emissions (denoted A′ and B′). The slopes between

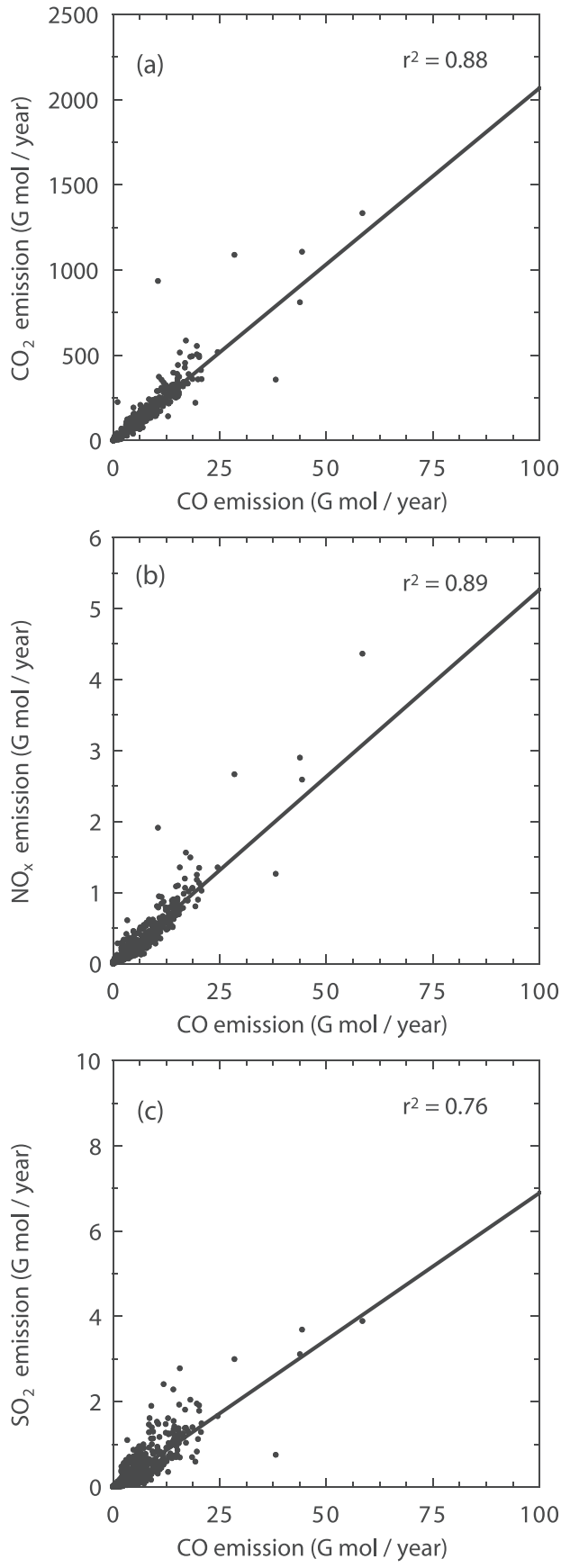

A and A′ and between B and B′ are equal to the emission ratio, E_{CO}/E_{CO2} from the second assumption. Consider that air mass C′ is produced by the mixing of A′ and B′ with the same ratio of mixing as when C is produced from A and B. The difference between C and C′ can be considered as the influence of anthropogenic emissions. Simple geometrical arguments show that the slope between C and C′ is equal to the slope for AA′, thus equal to the emission ratio E_{CO}/E_{CO2}. Consequently, once C′ is obtained from observations, a unique background value C can be calculated for this particular air mass as the interceptions between the background linear relationship (assumption 1) and a line thorough C′ with E_{CO}/E_{CO2} as its slope (assumption 2). Values of ΔCO and ΔCO_2 can then be calculated from the difference between values in air masses C and C′. Note that C′ can be considered either as resulting from mixing between A′ and B′ or as resulting from directly adding anthropogenic emissions to the background air mass C. Because of the linearity of the mixing process, a unique background value can be determined for an air mass that has experienced multiple mixing and multiple injection processes.

[22] The method to calculate the transport efficiency of NO_y is now described using Figure 5b where a measured data point is denoted as C′. We assume again that NO_y and CO values in background air masses have a linear relationship and that a ratio of enhancement following emissions can be expressed by an emission ratio, E_{NOx}/E_{CO}. Because we know the ΔCO (and, therefore, the background value of CO) value for this air mass from the CO-CO_2 correlation (Figure 5a), we can calculate a background value of NO_y (NO_y value in air mass C). The expected NO_y value due to inputs of anthropogenic emissions (NO_y value in air mass expected-C′ in Figure 5b) can then be calculated using E_{NOx}/E_{CO}. The measured NO_y would have been at this expected NO_y value if NO_y were to behave as a passive tracer. The observed NO_y value (NO_y value in air mass C′), however, can be lower than the value in air mass expected-C′, because of the loss of NO_y. The ΔNO_y value is defined by the difference between the observed value (C′) and background value (C). The transport efficiency of NO_y, $\varepsilon(NO_y)$, is defined as in equation (1), which is obtained from the ratio of ΔNO_y to the expected increase in NO_y (the difference between C and expected-C′). Note that the NO_y value in an observed air mass can be even lower than the "background relationship line" in the NO_y-CO diagram, as shown as air mass C″ in Figure 5b. Even in this case, the ΔNO_y value is still positive when the background value of this air mass (C) is lower than the observed value C″.

[23] In the same way, the transport efficiency of SO_x, $\varepsilon(SO_x)$, can be calculated. Note that if CO_2 is used as a reference gas to calculate the transport efficiency defined by equations (1) and (2) instead of using CO, the same

Figure 4. (opposite) Scatter plot between anthropogenic emissions (1° × 1° gridded data) in the region of 25°N–50°N and 100°E–130°E, except for South Korea (30°N–38°N and 126°E–130°E). This region covers mainly industrial regions in the northeastern part of China. Ratios of total emission amounts in this region (Table 2) are also shown by solid lines. These ratios were used as E_{CO}/E_{CO2}, E_{NOx}/E_{CO}, and E_{SO2}/E_{CO} in the present analyses.

Table 2. Emission and Emission Ratio of CO, CO_2, NO_x, and SO_2

Species	Area	Amount, tera-mol/yr	Ratio to CO, mol/mol
CO	northeastern China[a]	3.08	1
	South Korea	0.101	1
	Japan	0.243	1
CO_2	northeastern China	63.7	20.7
	South Korea	9.35	92.7
	Japan	27.3	112
NO_x	northeastern China	0.162	0.0527
	South Korea	0.0287	0.285
	Japan	0.0478	0.197
SO_2	northeastern China	0.212	0.0690
	South Korea	0.0129	0.128
	Japan	0.0125	0.0515

[a]Northeastern China defined in this study is the region of 25°N–50°N and 100°E–130°E except for South Korea.

result is obtained. This is because ΔCO and ΔCO_2 are interconnected as $\Delta CO/\Delta CO_2 = E_{CO}/E_{CO2}$.

[24] In our approach we assume the background relationship does not change, even when a loss of NO_y or SO_x takes place and a decrease in NO_y or SO_x (the difference between expected-C′ and C′) is attributed to a loss within anthropogenically injected NO_y or SO_x. In reality, however, NO_y or SO_x molecules, belonging to background air masses are also lost simultaneously when a loss process takes place. Consequently, the transport efficiency estimated by this approach is considered a lower limit. In the case of $\varepsilon(NO_y)$ estimation, lightning NO production and aircraft emissions can cause an overestimation and these effects will be addressed in section 5.7.

[25] An advantage of this method is that it can be used under the condition of multiple mixing, multiple injection, and multiple loss processes. Although we cannot tell when NO_y or SO_x is lost, we can calculate the fraction of net loss. The first key to this method is that instead of using a single value of CO or CO_2 as the background, we use a linear relationship between CO and CO_2 in background air masses, which covers certain ranges of CO and CO_2, to derive ΔCO. The other key is the use of emission ratios to estimate background values. In the next section, a determination of the background relationships is described.

4.2. Background Relationships

[26] In Figures 6a–6d, vertical profiles of CO, CO_2, NO_y, and SO_x (=SO_2 + nssSO_4^{2-}) observed from the P-3B aircraft are plotted using potential temperature as the vertical coordinate. For these figures, all data points obtained at west of 155°E are used irrespective of the latitude (17°N–42°N) except for those possibly influenced by a volcano on Miyakejima Island. Minimum values of CO, CO_2, and NO_y at each potential temperature level change smoothly with potential temperature. The solid line in each figure is a polynomial fit calculated for minimum values at each potential temperature level, and they will be referred to as "minimum value lines." Considering the fact that all of the air masses sampled in our study area had been transported from the Asian continent, these minimum values suggest the background levels of these species. Note that the minimum value at each potential temperature surface changes little with latitude. When geometric altitude is used instead of potential temperature, the minimum values change with latitude because of air mass motions along isentropic surfaces [*Koike et al.*, 1997]. In the case of SO_x, the background level was suggested to be close to zero because very low concentrations were frequently observed.

[27] In Figure 7a, a scatter plot between CO and CO_2 is shown using "continental air mass" data. In this plot, the color was coded using the altitude at which the air mass was sampled. From Figures 6a and 6b, pairs of CO and CO_2 values on the "minimum value lines" were calculated at various potential temperature levels between 280 and 310 K (open squares in Figures 6a and 6b), and they are also plotted in Figure 7a using open squares. As seen in this figure, these "minimum values" are linearly correlated within this CO and CO_2 range. Using the argument that these "minimum values" suggest the background levels of CO and CO_2, we use this relationship as the "background relationship" between CO and CO_2.

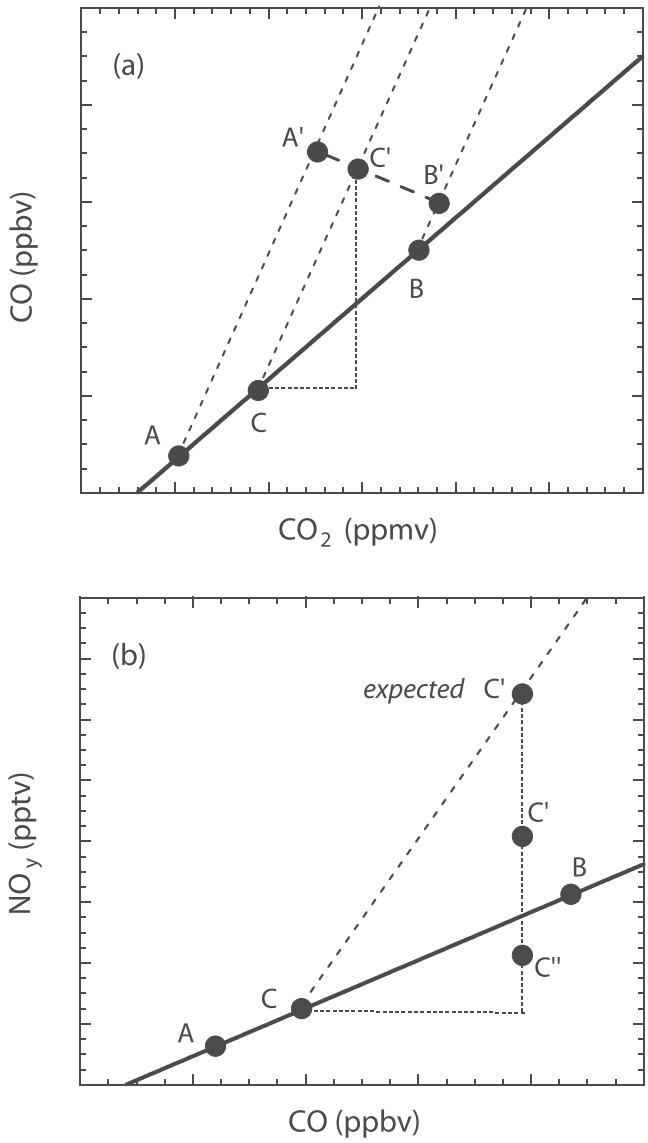

Figure 5. Schematic diagrams showing the procedure to derive background values (C) from observations (C′ or C″).

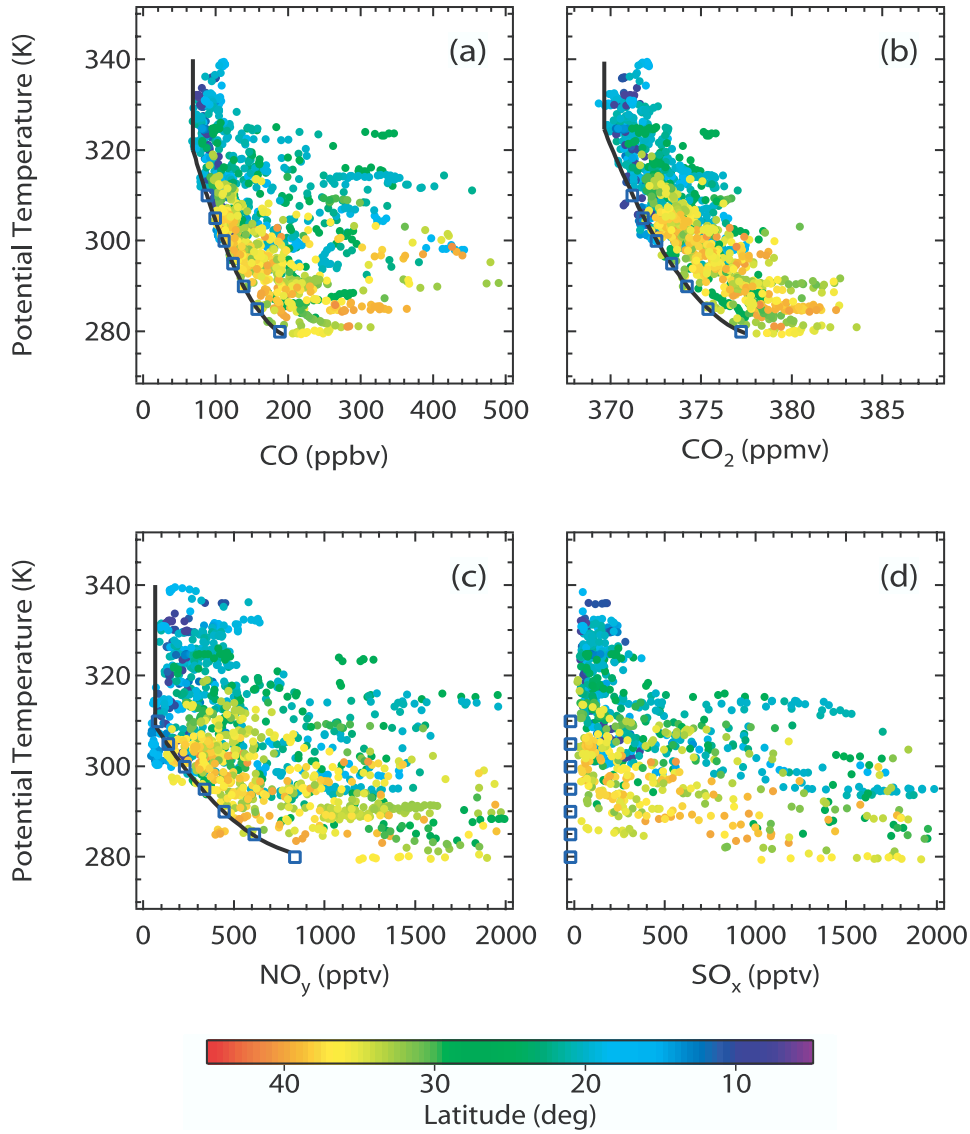

Figure 6. Vertical profiles of CO, CO_2, NO_y, and SO_x (=SO_2 + nssSO_4^{2-}). All of the P-3B data obtained at west of 155°E are used irrespective of the latitude (17°N–42°N) except for those possibly influenced by a volcano on Miyakejima Island. Potential temperature is used as the vertical coordinate. A solid line in each figure is a polynomial fit calculated for minimum values at each potential temperature level and is referred to as "minimum value line" in the text.

[28] As seen in Figure 7a, many data points are distributed around the "background relationship" line. Vertical profiles of CO and CO_2 suggest that these air masses have chemical characteristics of a background air mass, which is influenced little by anthropogenic sources over the East Asia. This is further confirmed using a correlation with Halon 1211 (CF_2ClBr) and OCS as described below. In Figures 7b and 7c, scatter plots between CO and CO_2 are shown and levels of Halon 1211 and OCS are used for color-coding. Halon 1211 is considered to be a unique tracer for Chinese urban emissions [*Blake et al.*, 2001; *Blake et al.*, 2003] because China is currently responsible for about 90% of the world's production following regulation by the Montreal Protocol [*Fraser et al.*, 1999]. It is used in fire extinguishers and its residence time in the atmosphere is 10 to 20 years. OCS has also been found to be a good indicator of anthropogenic emission from China and likely originates from coal burning (J. Green et al., manuscript in preparation, 2003). Coal combustion is a dominant contributor to both CO_2 and SO_2 emission in China [*Streets et al.*, 2003]. The global average residence time of OCS was estimated to be about 4 years [*Chin and Davis*, 1995]. As seen in Figures 7b and 7c, both Halon 1211 and OCS values in air masses above the "background relationship" are systematically higher than those in air masses around the "background relationship." This result indicates that air masses around the "background relationship" were influenced little by anthropogenic emissions over China.

[29] In summary, the "background relationship" between CO and CO_2 shown in Figure 7a was established using the t10 minimum values at each potential temperature level observed in our study area. The correlations with both

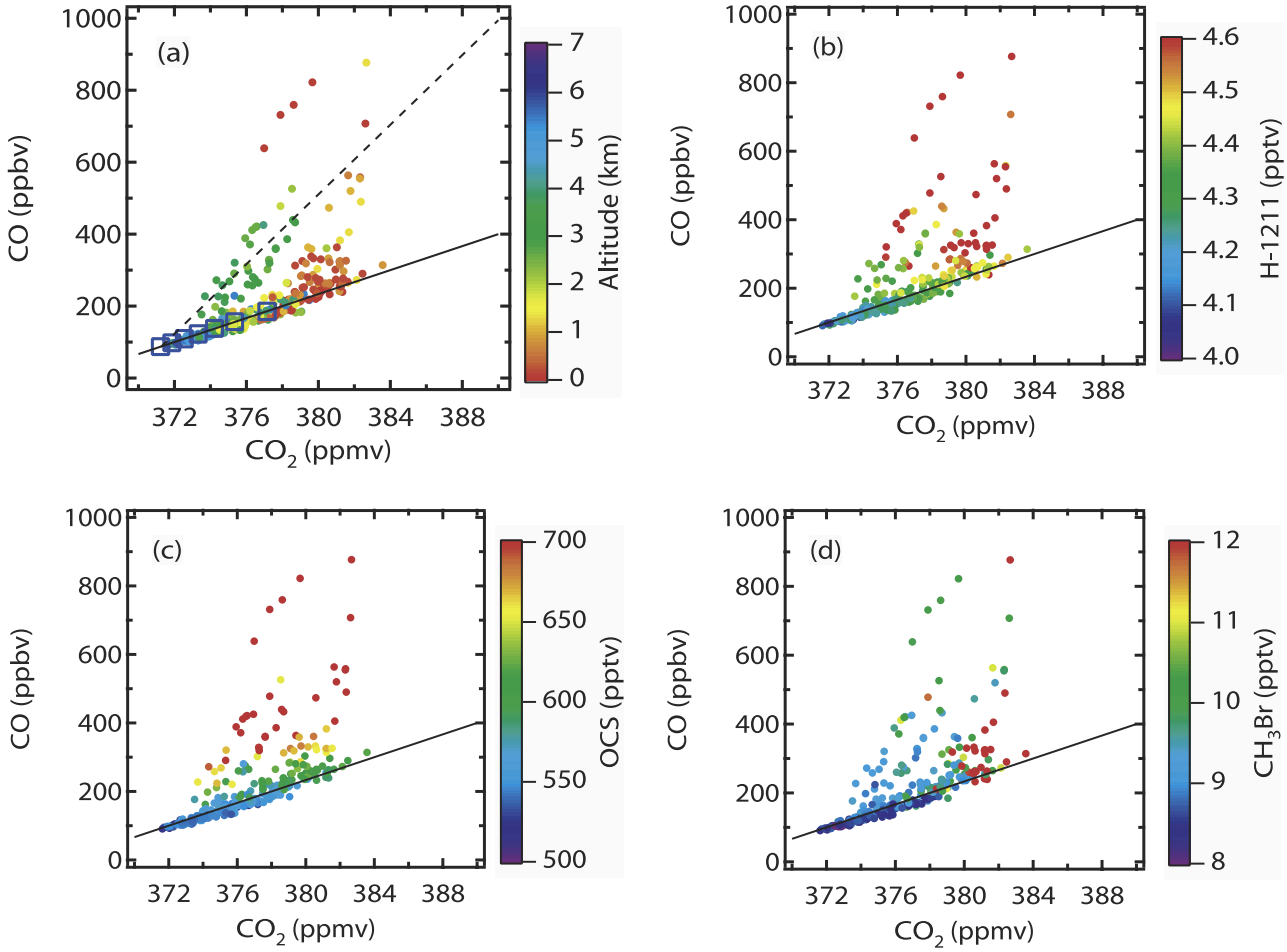

Figure 7. Scatter plot between CO and CO_2 in "continental air masses," which were sampled at 30°N–42°N and 124°E–140°E (P-3B data). Color was coded using (a) sampling altitude, (b) Halon 1211 mixing ratio, (c) OCS mixing ratio, and (d) CH_3Br mixing ratio. Open squares show pairs of CO and CO_2 values on the "minimum value lines" shown in Figures 6a and 6b. A solid line is a least squares fit to these open squares, and it will be referred to as "background relationship" in the text. The dashed line denotes the emission ratio of CO relative to CO_2 (E_{CO}/E_{CO2}) in the northeastern part of China (Table 2).

Halon 1211 and OCS confirm the validity of the use of this relationship as the "background relationship." In this study, one common "background relationship" is defined for the boundary layer air and free tropospheric air. Thus transport efficiency can be calculated even when an air masses in the boundary layer and free troposphere are mixed together. The degree of influence from anthropogenic emissions can be estimated by the value of ΔCO, irrespective of the altitude.

[30] Influences from Japanese and South Korean sources are noted here. In Figure 7d, a scatter plot between CO and CO_2 is shown using methyl bromide (CH_3Br) for color-coding. During TRACE-P, enhancements of CH_3Br were found in air masses when they had been advected over Japanese and South Korean ports, suggesting that it can be used as a unique tracer for influences from these two countries [*Blake et al.*, 2003]. High levels of CH_3Br are found in air masses in which CO and CO_2 was greater than 200 ppbv and 380 ppmv, respectively as shown in Figure 7d. These air masses are found around the "background relationship" and this is consistent with the fact that emission ratios E_{CO}/E_{CO2} over Japan and South Korea are systematically lower than that over China and are closer to a slope of "background relationship" (Table 2). These results suggest that Japanese and South Korean sources had only small influences in estimating ΔCO values.

[31] The "background relationship" between NO_y and CO was calculated in the same way, using "minimum value lines" shown in Figures 6a and 6c. This relationship is shown as a solid line in a scatter plot between NO_y and CO (Figure 8a). Black squares in this figure denote low-ΔCO air masses (ΔCO < 30 ppbv) in which CO and CO_2 values are close to the CO-CO_2 background relationship line. As seen in this figure, most of the low-ΔCO data correspond to data points around the "background relationship" between NO_y and CO. Although clear increases in NO_y are seen in some low-ΔCO air masses sampled at low altitudes, they were likely due to influences from Japanese and/or South Korean sources (relatively high CH_3Br concentrations as seen in Figure 7d) and a number of data is limited. Consequently, the method to estimate the transport efficiency described in the previous section can be applied to NO_y. In the case of SO_x, the background level was chosen to be zero, as described above. However, there is a positive correlation between SO_x and CO in low-ΔCO air masses, and mixing

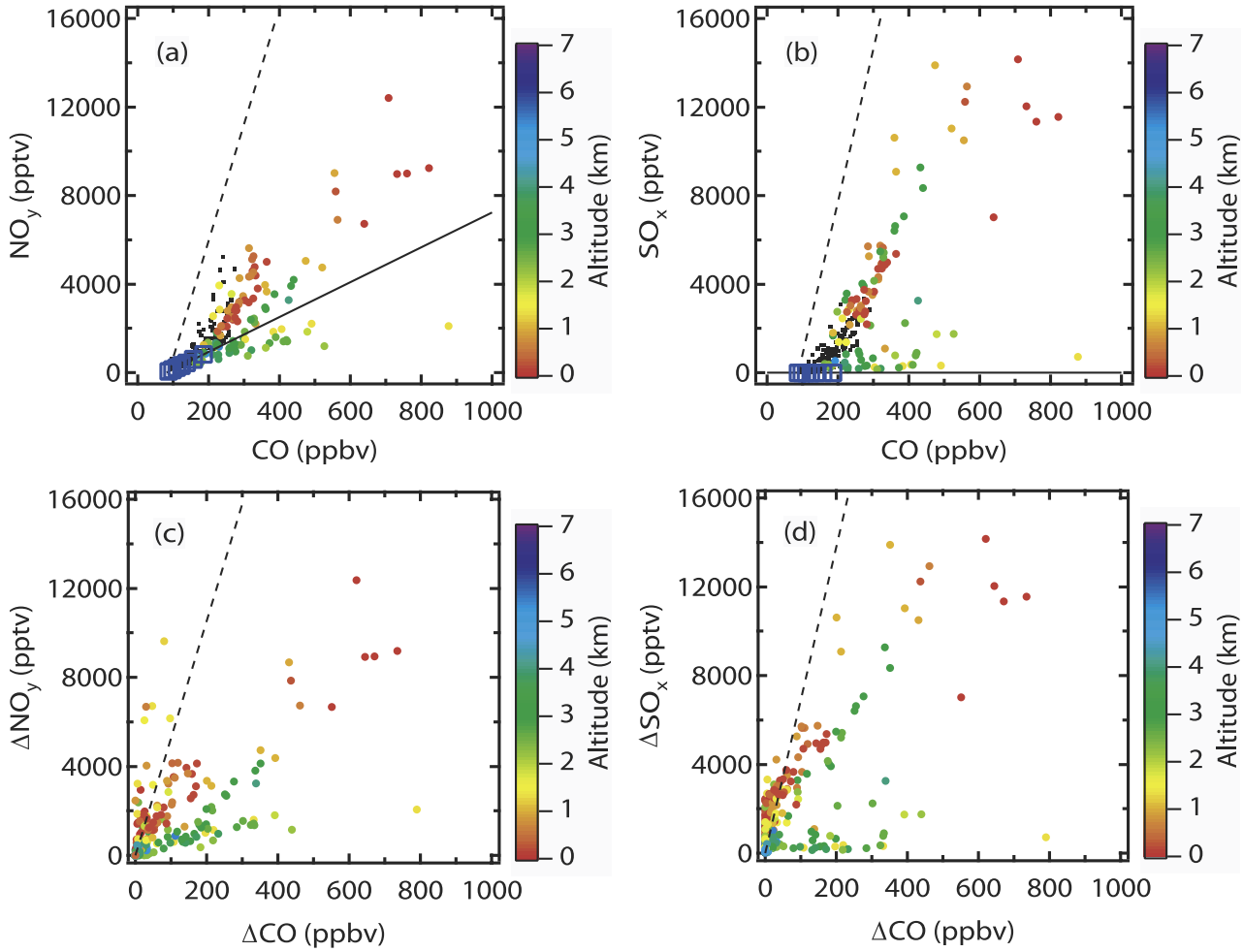

Figure 8. Scatter plots between (a) NO_y and CO, (b) SO_x and CO, (c) ΔNO_y and ΔCO, and (d) ΔSO_x and ΔCO in "continental air masses" (P-3B data). ΔSO_x values are identical to SO_x values because a zero background was assumed. Open squares show pairs of NO_y and CO or SO_x and CO values on the "minimum value lines" shown in Figures 6a, 6c, and 6d. A solid line and dashed line denote the "background relationship" and the emission ratio (E_{NOx}/E_{CO} or E_{SOx}/E_{CO}) in the northeastern part of China (Table 2), respectively. Black squares denote air masses in which $\Delta CO < 30$ ppbv.

with background air masses could result in some errors in our estimation (Figure 8b). We note that ΔCO values are estimated more accurately than ΔNO_y and ΔSO_x values in this study. The accuracy of the background level determination is more important for CO because the relative variability in CO due to anthropogenic emissions is smaller as compared with that in NO_y [*Parrish et al.*, 1991; *Stohl et al.*, 2002].

[32] Finally, it is noted that if an emission ratio E_{CO}/E_{CO2} is similar to a slope of the "background relationship" between CO and CO_2, influences cannot be extract using the present method. As described above, this is the case for emissions from Japan and South Korea. High E_{CO}/E_{CO2} ratios of Chinese emissions enable us to evaluate their impact.

5. Results and Discussion

5.1. Episodes of High-ΔCO Events

[33] In the statistical analyses described in the following sections, we only used air masses in which ΔCO values were greater than 30 ppbv (i.e., air masses clearly influenced by anthropogenic sources over the northeastern part of China). A threshold value of 30 ppbv was subjectively chosen by assuming a symmetrical distribution of ΔCO values in background air masses around the $\Delta CO = 0$ line ("background relationship" line in Figures 7a–7d). Air masses in which $\Delta CO > 30$ ppbv consisted of 30% of "continental air masses," and this fraction is higher at 0–2 km as compared with that at 2–7 km. Locations where these air masses were sampled are shown in Figure 1. After this selection, 19–42 and 9–29 data points remain in "continental" and "Chinese" air masses, respectively, in each of the 0–1, 1–2, and 2–4 km altitude ranges, while only 2 and 1 data points remain in these two air masses in the 4–7 km range. Results at 4–7 km likely do not represent the average in the western Pacific region. Uncertainties in the estimation at 4–7 km altitude range are discussed in section 5.5.

5.2. Correlation

[34] In Figure 8a, a scatter plot between CO and NO_y is shown using all of the "continental air mass" data. As seen in this figure, enhancements in NO_y are positively

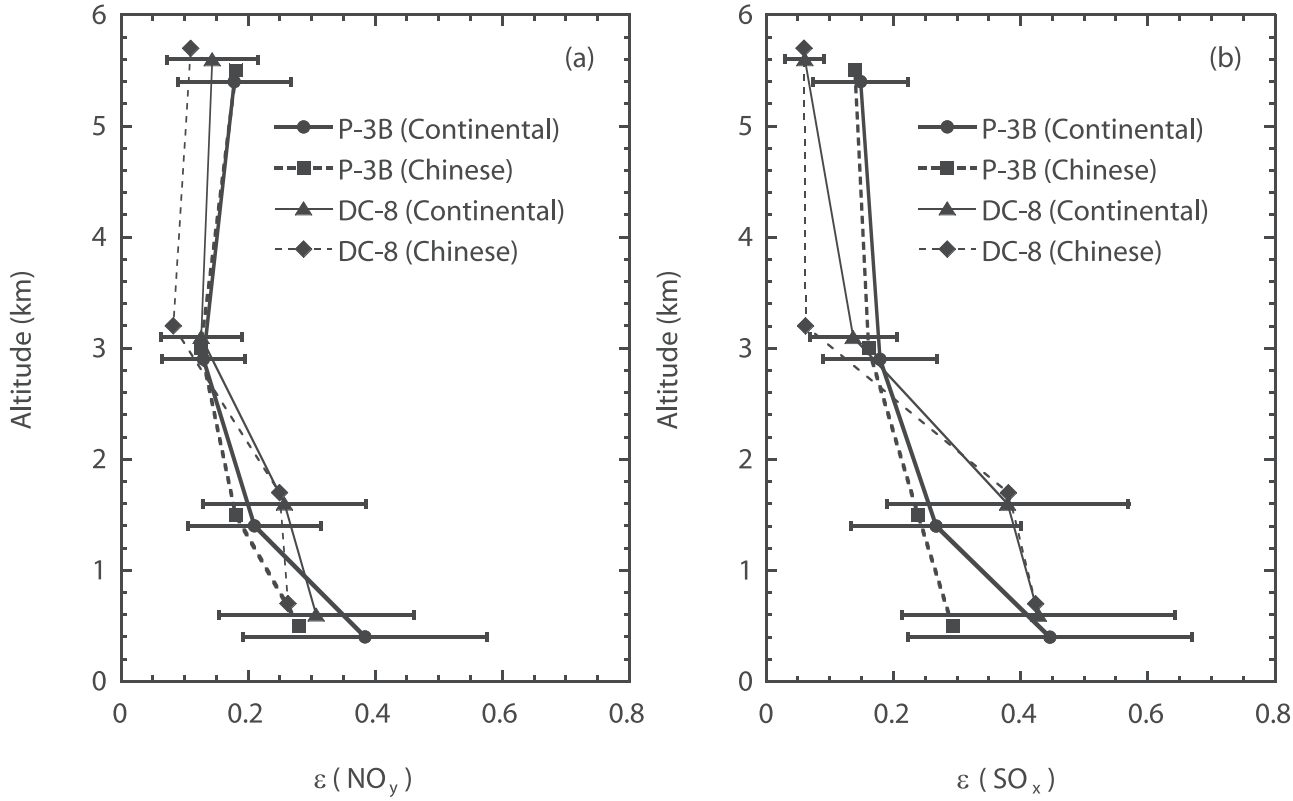

Figure 9. Vertical profiles of the transport efficiency for (a) NO_y, defined in equation (1) and (b) SO_x ($=SO_2 + nssSO_4^{2-}$), defined in equation (2). Values of ΔCO, ΔNO_y, and ΔSO_x were averaged (only using air masses in which $\Delta CO > 30$ ppbv) before taking their ratios. Emission ratios, given in Table 2 were used. Horizontal bars indicate uncertainties in the estimations (50% range).

correlated with those in CO, suggesting that these NO_y enhancements were due to anthropogenic emissions. The enhancement was greatest at altitudes below 2 km. A clear positive correlation between NO_y and CO, suggesting anthropogenic influences, was also found in the lower and middle troposphere over the western Pacific in February–April 1994, during PEM-West B [*Koike et al.*, 1997].

[35] In Figure 8c, a scatter plot between ΔNO_y and ΔCO is shown for "continental air mass" data. The relationship between ΔNO_y and ΔCO is similar to that between NO_y and CO (Figure 8a) because background values of individual data are not very different. The ΔNO_y and ΔCO are positively correlated; however, the slope is lower than the emission ratio, suggesting that anthropogenically emitted nitrogen compounds had been removed from the air masses before they were sampled from the P3-B aircraft. Ratios of increases, $\Delta NO_y/\Delta CO$, are generally higher at altitudes below 2 km as compared to those at higher altitudes, suggesting removal of NO_y during the vertical transport. On the other hand, ratios of increases in air masses in which ΔNO_y and ΔCO values are very high ($\Delta NO_y > 6$ ppbv and $\Delta CO > 400$ ppbv) are similar to those of other air masses. These air masses are considered to have been influenced by anthropogenic sources more strongly, however the removal rate is similar to those of less-influenced air masses.

[36] It is noted that there are some data which have greater $\Delta NO_y/\Delta CO$ ratios than the E_{NO_x}/E_{CO} ratio. This is likely due to inhomogeneity in emission ratios and/or influences from Japanese and/or South Korean emissions. Most of these data points are found in air masses in which $\Delta CO < 30$ ppbv and therefore, they were discarded in the following statistical analyses as described in section 5.1.

[37] In Figure 8b, a scatter plot between CO and SO_x is shown using "continental air mass" data. A clear correlation was found between the two values, especially at altitudes below 2 km. A positive correlation is also seen in a scatter plot between ΔCO and ΔSO_x (Figure 8d). As for NO_y, the slope was lower than the emission ratio, E_{SO2}/E_{CO}, suggesting the removal of SO_x. Air masses sampled at 2–7 km appear to belong to two groups. In one of the groups, the slope of the increase is similar to that of the 0–2 km data, while very little increase of SO_x is found in the other group. These two groups of air masses were sampled during different flights (mostly from flights 13 and 19);

Table 3. Transport Efficiency of Reactive Nitrogen[a]

	P-3B			DC-8
	$\varepsilon(NO_y)$	$\varepsilon(NO_x)$	$\varepsilon(NO_3^-)$	$\varepsilon(NO_y)$
4–7 km	0.18 (0.18)	0.004	0.001	0.14 (0.11)
2–4 km	0.13 (0.13)	0.007	0.001	0.13 (0.08)
1–2 km	0.21 (0.18)	0.013	0.025	0.26 (0.25)
0–1 km	0.38 (0.28)	0.048	0.16	0.31 (0.26)

[a]Results are for air masses in which $\Delta CO > 30$ ppbv within "continental air masses." Values in parentheses are for "Chinese air masses."

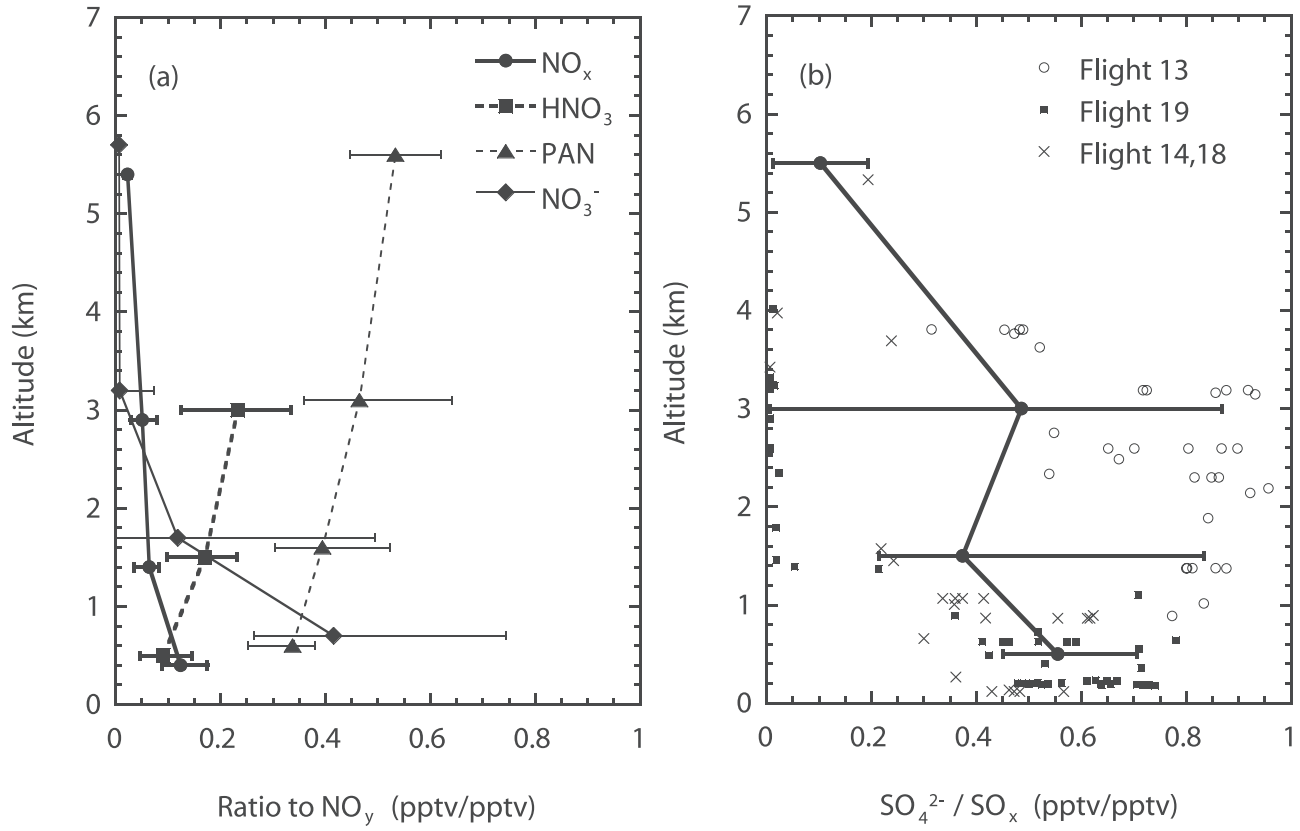

Figure 10. (a) Vertical profile of the partitioning within the NO_y species (P-3B data). Median values and 67% ranges (horizontal bars) in "continental air masses" (and $\Delta CO > 30$ ppbv) are shown. (b) Vertical profile of $nssSO_4^{2-}/SO_x$ ratio (P-3B data). Median values and 67% ranges (horizontal bars) in "continental air masses" (and $\Delta CO > 30$ ppbv) are shown. Individual data points are also shown.

however, many of these air masses had been transported from below 800 hPa over the northeastern part of China. Consequently, the observed difference in the transport efficiency was largely due to differences in the transport processes, in which the degree of loss of SO_2 and/or $nssSO_4^{2-}$ was different (more discussion on flight 19 data is given in section 5.4.).

5.3. Vertical Profile of $\varepsilon(NO_y)$

[38] Average ΔCO and ΔNO_y values in "continental air mass" data were calculated within each altitude range (0–1, 1–2, 2–4, and 4–7 km), and the transport efficiency, $\overline{\varepsilon(NO_y)}$, was calculated using these averages ($\overline{\Delta NO_y}$ and $\overline{\Delta CO}$). In this calculation, we only used data with $\Delta CO >$ 30 ppbv. We took the ratio of the average rather than using the median value of individual ratios because events in which ΔCO and ΔNO_y were large should have a greater impact on the overall efficiency of the transport. It has been reported that the majority of transport of pollutants from the Asian continent to the Pacific Ocean is generally the result of episodic events rather than continuous steady flow [*Bey et al.*, 2001; *Liu et al.*, 2003; *Jaffe et al.*, 1999]. We note that the choice of the threshold value of ΔCO (>30 ppbv) is not very sensitive to the results because the averages are used instead of using the medians.

[39] A vertical profile of the average transport efficiency in the "continental air" is shown in Figure 9a (Table 3). In this figure, the transport efficiency calculated using only "Chinese air masses" is also shown. "Chinese air masses" were those that passed over China at altitudes below the 800-hPa level (boundary layer) within 5 days prior to measurement without passing over South Korea or Japan at these low altitudes, as described in section 3.1. We note that when air masses in which $\Delta CO > 30$ ppbv are selected, Chinese air masses in each altitude range consist of 20–70% of the continental air masses. As seen in Figure 9a, a transport efficiency of 20–40% was found at 0–2 km. "Chinese air masses" at 0–2 km were mostly sampled over the Yellow Sea, and they were sampled within 24 hours after they had left the coast of China. The efficiency estimated in this study indicates that 60–80% of NO_y had already been removed in the source region before these air masses left the continent, although additional loss could have also occurred during this short transport over the ocean. The efficiency tends to be lower at higher altitudes, and values of about 15% were found at 2–7 km. The lower efficiency in the free troposphere suggests that HNO_3 and NO_3^- were removed by wet deposition during the vertical transport because precipitation is often accompanied by convection and synoptic-scale air mass lifting in association with cold frontal systems, which is known as the warm conveyer belt (WCB). The removal process is examined more quantitatively below.

[40] In Figure 10a, vertical profiles of median values of HNO_3/NO_y and NO_3^-/NO_y in "continental air masses" are shown. These values are also given in Table 4. For this

Table 4. Partitioning Within NO_y and SO_x (P-3B)[a]

	NO_y				SO_x
	NO_x/NO_y	PAN/NO_y	HNO_3/NO_y	NO_3^-/NO_y	$nssSO_4^{2-}/SO_x$
4–7 km	0.023	0.53	–	0.0066	0.10
2–4 km	0.051 (0.028–0.078)	0.46 (0.36–0.64)	0.23 (0.12–0.33)	0.0078 (0.0015–0.0723)	0.49 (0.01–0.87)
1–2 km	0.064 (0.036–0.083)	0.39 (0.30–0.52)	0.17 (0.10–0.23)	0.12 (0.00–0.49)	0.37 (0.21–0.83)
0–1 km	0.12 (0.09–0.17)	0.34 (0.25–0.38)	0.091 (0.046–0.146)	0.42 (0.26–0.74)	0.56 (0.45–0.71)

[a]Median values for air masses in which $\Delta CO > 30$ ppbv within "continental air masses." Values in parentheses are 67% ranges.

calculation, we only used data with $\Delta CO > 30$ ppbv. As seen in this figure, $HNO_3 + NO_3^-$ accounts for 50% and 30% of NO_y at 0–1 and 1–2 km, respectively. Henry's law equilibrium and laboratory studies of HNO_3 uptake on ice surfaces indicate that HNO_3 is ~100% fractionated into the condensed phase in both warm and glaciated clouds [*Mari et al.*, 2000, and references therein]. One-dimensional model calculations for tropical continental deep convection suggest that about 80% of HNO_3 was scavenged during vertical transport [*Mari et al.*, 2000]. Similarly, very low NO_3^-/NO_y values of 0.007 in the free troposphere, as compared with those observed in the boundary layer of 0.1–0.4, indicate that nitrate aerosols were also scavenged quite efficiently during vertical transport. In fact, ammonium nitrate (NH_4NO_3), which is generally seen in accumulation mode aerosol and which is considered to have been measured by the NO_y instrument, is expected to be efficiently scavenged by cloud droplets. Assuming 100% removal of HNO_3 and NO_3^- aerosols in the boundary layer during vertical transport into the free troposphere, the factor of 2 reduction of $\varepsilon(NO_y)$ estimated in this study can be explained. Formation of HNO_3 from NO_x during and after vertical transport retains the HNO_3/NO_y ratios in the free troposphere, while very low NO_3^-/NO_y ratios in the free troposphere suggest that the formation of nitrate aerosol was likely limited because an insufficient amount of NH_3 was available to neutralize the acidity.

[41] The transport efficiency of NO_y during the TRACE-P period was also studied by *Miyazaki et al.* [2003]. Although a single value was used for the background levels of NO_y and CO in their analysis, generally similar results were obtained: 30% and 10–20% in the boundary layer and free troposphere, respectively. Synoptic-scale WCB and convection were found to be important mechanisms for the transport of anthropogenic reactive nitrogen to the free troposphere. The transport efficiency of NO_y from North America was studied by *Stohl et al.* [2002] using North Atlantic Regional Experiment (NARE) 1996 and 1997 data. They used CO and Lagrangian tracers as a reference and found that only 3–5% of NO_y emissions reached altitudes above 3 km. D. D. Parrish et al. (Relation of NO_y and CO concentrations in the free troposphere: Fraction and composition of NO_y transported in polluted air masses lofted from the North American continental boundary layer, submitted to *Journal of Geophysical Research*, 2003) also studied the relationship between NO_y and CO using five field campaigns over the North America (summer season) and the western North Atlantic Ocean (spring and fall) and the NO_y transport efficiencies in the free troposphere are estimated to have been 10–30%.

[42] Vertical profiles of the partitioning of reactive nitrogen (Figure 10a and Table 4) show that PAN was the dominant species in "continental air masses" ($\Delta CO > 30$ ppbv). Because of the long lifetime of PAN at low temperatures in the free troposphere, PAN would be transported farther downwind and eventually produce NO_x after descending to lower altitudes [e.g., *Moxim et al.*, 1996; *Koike et al.*, 1997]. Consequently, this fraction is considered as a potential source of NO_x. Direct transport of NO_x, however, was found to be very limited. The NO_x/NO_y ratio was 0.06–0.12 and 0.02–0.05 at 0–2 km and 2–7 km, respectively (Figure 10a and Table 4). When $\varepsilon(NO_y)$ values in Table 3 (Figure 9a) are used, the transport efficiency of NO_x, $\varepsilon(NO_x)$, was calculated to be about 1–5% and 0.5% in the boundary layer and free

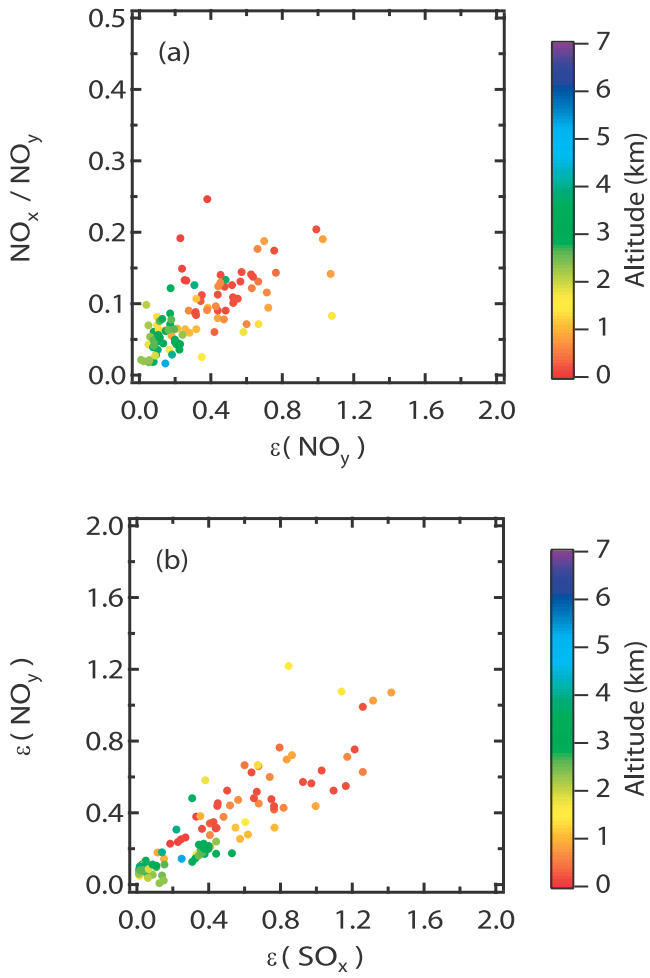

Figure 11. Scatter plot between (a) NO_x/NO_y and transport efficiency of NO_y, and (b) transport efficiencies of NO_y and SO_x (P-3B data). Air masses in which $\Delta CO > 30$ ppbv within "continental air masses" are used.

Table 5. Transport Efficiency of SO_x[a]

	P-3B		DC-8
	$\varepsilon(SO_x)$	$\varepsilon(nssSO_4^{2-})$	$\varepsilon(SO_x)$
4–7 km	0.15 (0.14)	0.015	0.06 (0.06)
2–4 km	0.18 (0.16)	0.087	0.14 (0.06)
1–2 km	0.27 (0.24)	0.10	0.38 (0.38)
0–1 km	0.45 (0.29)	0.25	0.43 (0.42)

[a]Results are for air masses in which $\Delta CO > 30$ ppbv within "continental air masses." Values in parentheses are for "Chinese air masses."

troposphere, respectively. This result means that only 0.5% of anthropogenically emitted NO_x remained in the form of NO_x when these air masses were transported into the free troposphere. Values of NO_3^-/NO_y have large variability at 0–2 km, partly because the NO_3^- amount in aerosol is generally limited by the availability of NH_3. When median values of NO_3^-/NO_y are used, the formation efficiency of NO_3^-, $\varepsilon(NO_3^-)$, was calculated to be 3–16% and 0.1% in the boundary layer and free troposphere, respectively. This low yield in the free troposphere is due to the efficient scavenging of nitrate aerosol, as described above.

[43] A scatter plot between $\varepsilon(NO_y)$ and NO_x/NO_y is shown in Figure 11a. As seen in this figure, these two quantities are positively correlated. Part of the correlation is due to their vertical profiles; however, a correlation is seen even within the boundary layer data. Because the loss of HNO_3 and NO_3^- results in a higher NO_x/NO_y ratio, a positive correlation cannot be simply explained by this process. When an air mass remained or stagnated within the boundary layer for a longer time period, conversion from NO_x to HNO_3 by gas-phase reaction with OH and nighttime heterogeneous reaction through N_2O_5 proceed further, leading to a lower NO_x/NO_y ratio. Concurrently, the loss of HNO_3 and NO_3^- results in a lower $\varepsilon(NO_y)$. Furthermore, during vertical transport, we may expect an efficient conversion of NO_x to HNO_3 due to the relatively large amounts of OH from H_2O and wet surface area for heterogeneous reaction. The results presented in this study suggest that the transport efficiency was higher in air masses that spent less time in the boundary layer, though a very limited fraction of emitted NO_x can still be brought into the free troposphere.

5.4. Vertical Profile of $\varepsilon(SO_x)$

[44] Vertical profiles of the average transport efficiency of SO_x ($=SO_2 + nssSO_4^{2-}$), $\varepsilon(SO_x)$, in the "continental air masses" and "Chinese air masses" are shown in Figure 9b (Table 5). As for $\varepsilon(NO_y)$, averages of ΔSO_x and ΔCO in high-ΔCO air masses ($\Delta CO > 30$ ppbv) were calculated ($\overline{\Delta SO_x}$ and $\overline{\Delta CO}$), and their ratio was divided by the emission ratio given in Table 2. As a result, the transport efficiency at 0–2 km was estimated to be 25–45%. "Chinese air masses" at 0–2 km were mostly sampled over the Yellow Sea, and they were sampled within 24 hours after they had left the coast of China, as described above. The efficiency estimated in this study indicates that 55–75% of SO_x had already been removed in the source region before these air masses left the continent. The transport efficiency of 15% at 2–7 km is lower than that at 0–2 km, suggesting that SO_2 and $nssSO_4^{2-}$ were removed by wet deposition during vertical transport. One-dimensional model calculations for tropical continental deep convection suggest that about 30% of SO_2 was scavenged during vertical transport [*Mari et al.*, 2000]. Although this value is lower compared to the value of 80% for HNO_3 due to the low Henry's Law constant, $nssSO_4^{2-}$ particles are considered to have been scavenged quite efficiently within the cloud and precipitation leading to lower $\varepsilon(SO_x)$ values in the free troposphere.

[45] A vertical profile of median values of $nssSO_4^{2-}/SO_x$ ratio is shown in Figure 10b (and Table 4). At 0–1 km altitude, $nssSO_4^{2-}/SO_x$ ratios of about 0.6 were observed during each of the four fights, suggesting that the conversion from SO_2 to SO_4^{2-} had taken place quite efficiently near the source region. Ratios of $nssSO_4^{2-}/SO_x$ of about 0.3–0.7 were obtained from the ground-based measurements at Cheju Island in the East China Sea [*Carmichael et al.*, 1997] and Taean station in Korea facing the Yellow Sea [*Kim et al.*, 2001], which also suggest rapid conversion within the boundary layer. On the other hand, at 2–4 km, $nssSO_4^{2-}/SO_x$ ratios differ significantly between the flights. In air masses sampled over Japan Sea during flight 19, $nssSO_4^{2-}/SOx$ ratios were quite low (Figure 10b), while the $\varepsilon(SO_x)$ values were higher than those of the other flights. During this flight, the CO, SO_2, and NO_y values reached 300–400 ppbv, 5–9 ppbv, and 2–4 ppbv, respectively, at 3 km, suggesting a significant impact from anthropogenic emissions. Because $\varepsilon(SO_x)$ values at 2–4 km during this flight were close to those at 0–1 km, the observed low $nssSO_4^{2-}/SO_x$ ratios might have been due to a limited formation of $nssSO_4^{2-}$ particles, rather than the removal of $nssSO_4^{2-}$ particles. When a median value of $nssSO_4^{2-}/SO_x$ is used with the transport efficiency of SO_x, a formation efficiency of sulfate aerosol is estimated to be 10–25% and 2–9% at 0–2 km and 4–7 km, respectively. The efficiency in the free troposphere was higher than that of nitrate aerosol in the same altitude rage ($\varepsilon(NO_3^-) = 0.1\%$) likely because sulfate aerosols can be formed more easily in the free troposphere after removal during vertical transport.

[46] A scatter plot of the transport efficiencies for NO_y and SO_x is shown in Figure 11b. As seen in this figure, they are positively correlated, even within each altitude range. This result suggests that loss processes of NO_y and SO_x proceeded simultaneously.

5.5. Comparison With $\varepsilon(NO_y)$ and $\varepsilon(SO_x)$ Values Derived From DC-8 Data

[47] In this study, the P-3B aircraft data were used exclusively. However, because measurements of NO_x, PAN, HNO_3, SO_2, and SO_4^{2-} (particles with diameters smaller than 2.7 μm) were also made onboard the NASA/DC-8 during TRACE-P, we performed the same analyses using the DC-8 data set obtained in the study area defined for the present study (30°N–42°N and 124°E–140°E). For NO_y values, we summed the DC-8 observations of NO_x, PAN, and HNO_3. In HNO_3 measurements, particulate nitrate of diameters smaller than 1–2 μm is considered to have been measured with gas phase HNO_3. When we plot a $CO\text{-}CO_2$ scatter plot using Halon 1211 and OCS as markers of Chinese urban emissions, very similar results to those shown in Figures 7a–7c are obtained (not shown). The "background relationship" derived from the P-3B also fits the DC-8 data set well. This is partly because the same

research groups made measurements onboard the two aircraft for CO, CO_2, and species obtained from whole air sampling. In fact, very good agreement between the two sets of measurements was found during the P-3B/DC-8 intercomparison flights [*Eisele et al.*, 2003].

[48] Vertical profiles of $\varepsilon(NO_y)$ and $\varepsilon(SO_x)$ values derived from DC-8 "continental air" and "Chinese air" are shown in Figures 9a and 9b, together with the P-3B results. DC-8 "Chinese air masses" were selected using the same definition as that for P-3B data using air mass trajectories. These results are also summarized in Tables 3 and 5. As seen in the figure, most of the results obtained from measurements from the two aircraft agreed to within 50%. When only the transport efficiencies of SO_2 are compared, a similar degree of agreement was found at 0–2 km, although the P-3B values in the boundary layer and free troposphere were found to be lower and higher, respectively. Disagreement by a factor of 3 was found between the P-3B and DC-8 SO_2 measurements during the P-3B/DC-8 intercomparison flights [*Eisele et al.*, 2003]. However, the agreement in the estimates indicates that the results obtained in this study are robust.

[49] As described in section 5.1, only two samples of air masses, in which $\Delta CO > 30$ ppbv, were used for P-3B data analyses at 4–7 km (continental air masses), and therefore they do not represent the average in the western Pacific region. A number of data with $\Delta CO > 30$ ppbv is small at this altitude range, primarily due to a limited number of uplifting events. When a criterion of $\Delta CO > 5$ ppbv is used instead, 7 data (10% of the total number of data at 4–7 km) remain and $\varepsilon(NO_y)$ and $\varepsilon(SO_x)$ of 22 and 20% are obtained, suggesting a range of uncertainties in our estimations. Measurements at altitudes above 4 km were made more frequently by the DC-8. Although data above 7 km were also used for the DC-8 statistics, the agreement with the DC-8 estimates (within 25% and 85% for NO_y and SO_x, respectively) derived using a greater number of data (32 data) supports the validity of the results obtained from the P-3B data at 4–7 km (Tables 3 and 5).

5.6. Export Flux and Budget

[50] The transport efficiencies $\varepsilon(NO_y)$ and $\varepsilon(SO_x)$ defined in equations (1) and (2) were determined for individual air masses. The value of $\varepsilon(NO_y)$ was derived from the number density of observed NO_y in one air mass divided by the expected NO_y number density in that air mass assuming that there is no loss after anthropogenic input. Consequently, the efficiency can be 100% in individual air masses. In the next step, we estimated a time-averaged eastward flux of NO_y and SO_x across the 130°E meridional plane at 30°N–40°N during the TRACE-P period. Because of the limited air mass sampling frequency, only fractional contributions from various altitudes are considered. To estimate these quantities, we first examined an eastward flux of CO. The export flux fraction of CO is determined in this study as follows.

$$f_{CO}(z \sim z+\Delta z) = \frac{\int_z^{z+\Delta z} F_{air} \cdot \overline{\Delta CO} \cdot \gamma \cdot dz}{\int_0^{tropopause} F_{air} \cdot \overline{\Delta CO} \cdot \gamma \cdot dz}, \qquad (3)$$

where F_{air} is the eastward flux of air molecules at 130°E meridional plane at 30°N–40°N derived using ECMWF data. Here γ is the occurrence frequency of the events in which $\Delta CO > 30$ ppbv were observed from the P-3B aircraft. For $\overline{\Delta CO}$, averaged values in the continental air masses ($\Delta CO > 30$ ppbv) were used. These three quantities were determined as a function of altitude and calculations were made below 7 km, where P-3B data are available. Note that the occurrence frequency of pollution transport events (events in which $\Delta CO > 30$ ppbv) is highly dependent on where and when P-3B aircraft measurements were made, although only the relative frequency among the various altitude ranges was used for our estimation. Consequently, the flux estimated here should be considered as a case study for air masses which we sampled during TRACE-P. Using equation (3), it was found that 30% of CO export took place through the boundary layer (0–2 km) and 70% was transported through the free troposphere (2–7 km). Although the size of the ΔCO value was similar at altitudes below 4 km, higher wind speeds resulted in a greater flux in the free troposphere. The CO flux within each 1-km layer was suggested to be greatest in the 2–4-km altitude range. This result is consistent with the GEOS-CHEM model for the PEM-West B period (February–March 1994) shown by *Bey et al.* [2001]. *Liu et al.* [2003] also showed similar results for the TRACE-P period. When we attempted to estimate the absolute value of the averaged eastward flux of CO instead of the fractional contributions, values of $1–3 \times 10^{-9}$ mol cm^{-2} s^{-1} were obtained at altitudes below 4 km. This is again in reasonable agreement with the results obtained by *Liu et al.* [2003].

[51] The export flux fraction of NO_y is determined in the similar way.

$$f_{NOy}(z \sim z+\Delta z) = \frac{\int_z^{z+\Delta Z} F_{air} \cdot \overline{\Delta NO_y} \cdot \gamma \cdot dz}{(E_{NOx}/E_{CO}) \cdot \int_0^{tropopause} F_{air} \cdot \overline{\Delta CO} \cdot \gamma \cdot dz}, \qquad (4)$$

The denominator is the expected total flux of NO_y molecules that could have crossed the meridional plane, assuming that there is no loss after receiving anthropogenic emissions. The numerator is the observed flux of NO_y molecules that actually crossed the meridional plane within each altitude range (continental air masses in which $\Delta CO > 30$ ppbv). The export flux fraction can be considered as a weighted average of the transport efficiency for which air flux and occurrence frequency of pollution transport event are used as a weighting function. Using equation (4), the export flux fraction of NO_y at 0–7 km during TRACE-P was estimated to be 18%. About half (8%) of the export flux took place through the boundary layer and the other half (10%) took place through the free troposphere. Similarly, the export flux fraction of SO_x at 0–2 km and 2–7 km was estimated to be 10% and 12%, respectively. The fact that export flux fractions were similar between the two altitude ranges for NO_y and SO_x is in contrast to the case of CO, in which the fraction in the free troposphere was greater as described above. The free tropospheric fraction was less significant for NO_y and SO_x because loss during the vertical transport resulted in lower $\varepsilon(NO_y)$ and $\varepsilon(SO_x)$ values. The flux in the free troposphere is important for long-range transport, due to greater wind speeds and less-frequent

removal, while the flux in the boundary layer suggests an impact on neighboring countries, such as Japan.

[52] The budget of NO_y and SO_x (total export flux versus emissions) over the East Asia region is also examined here. During TRACE-P, predominant westerly flow generally brought air masses influenced by anthropogenic emissions over the East Asia into the western Pacific region. *Liu et al.* [2003] show using the GEOS-CHEM model that eastward fluxes of Asian CO is strongest at 30–45°N in the boundary layer and at 20–35°N in the lower free troposphere. The former mostly reflects anthropogenic emissions, while the latter includes contributions from both anthropogenic and biomass burning emissions. When we assume that a majority of air masses influenced by anthropogenic emissions is transported to 30–40°N (and sampled from the P-3B aircraft) or an export flux fraction is similar at other latitude ranges, we can use an estimate of export flux fraction as a budget estimate. This assumption may not be very unreasonable, because a total flux of CO at 30–40°N at 130°E meridional plane described above agrees with the total emission of CO at 25°N–50°N and 100°E–130°E (except for emissions from South Korea) within 20%. However considering the limitation of air mass sampling in space and time during TRACE-P, this budget analysis should be considered as a case study as for the flux analysis. The results of the export flux fraction obtained above suggest that of total number of molecules of NO_x and SO_2 emitted over the northeastern part of China, only 18 and 22% were transported out from the Asian continent into the western Pacific in air masses which we sampled during TRACE-P.

[53] Budget of NO_y and SO_x in the East Asia region has been estimated in various numerical model studies [e.g., *Bey et al.*, 2001; *Chin et al.*, 2000; *Tan et al.*, 2002]. Usually, the total export flux from a selected domain is calculated from the difference between the total source and total sink. *Bey et al.* [2001] showed using the GEOS-CHEM model for the PEM-West B period (February–March 1994) that about 70–80% of NO_x emitted in Asia was lost within the domain by deposition of HNO_3, and the net export flux was 20–30%, although the contribution from biomass burning in the southern part of China was also included in their model calculations. *Chin et al.* [2000] showed using the GOCART model that the export flux fraction of anthropogenic SO_x from eastern Asia was about 16%, with 2/3 of it as SO_2. Nearly half of the emitted SO_2 is lost by dry-deposition to the surface. *Tan et al.* [2002] showed using their three-dimensional (3-D) model calculations for the late winter/early spring period that about 50% of the anthropogenic SO_x emitted over East Asia was removed from the continental source regions. About 30% is further removed within the neighboring ocean (region west of about 155°E), and 20% is exported out of their model domain. The vast majority of the exported SO_x was in the form of sulfate aerosol. These estimates are generally consistent with those obtained in this study.

5.7. Uncertainties

[54] Uncertainties in the estimation of transport efficiency are affected by uncertainties in the emission data, biogenic sources of CO_2 [*Vay et al.*, 2003] which is not considered in this study, measurements imperfections, background relationships, the choice of the threshold value of ΔCO (30 ppbv), and loss of NO_y and SO_x in background air masses. Also, the two assumptions were made in our analyses: first, CO, CO_2, NO_y, and SO_x values in background air masses have a linear relationship, and second, the ratio of enhancements due to anthropogenic emissions is always the same. It is hard to evaluate individual uncertainties in a consistent manner, however we estimated an overall uncertainty in our estimation of transport efficiency to be on the order of 50% (horizontal bars in Figures 9a and 9b).

[55] Some specific sources of uncertainty are described here. First, *Palmer et al.* [2003] shows using an inverse model analysis that the anthropogenic emissions of CO in China estimated by *Streets et al.* [2003] is likely to be underestimated by 30%. When CO emissions are increased by 30% in our analyses, the transport efficiencies and the export flux fractions (equation (4)) increase by about 30%.

[56] Second, emissions from Japan and South Korea are examined. Emission ratios of CO, CO_2, and NO_x in Japan and South Korea are very different from those in China (Table 2), as described in section 3.2. Consequently, when an air mass is influenced by emissions over South Korea or Japan, the ratio of increase, $\Delta NO_y/\Delta CO$ and $\Delta SO_x/\Delta CO$, will be different from those expected from Chinese emissions. However, as shown in Figures 9a and 9b, results obtained using "continental air masses" generally agreed with those using "Chinese air masses". As explained in section 3.1, a more strict criterion on the air mass trajectories was applied to select "Chinese air masses," suggesting the robustness of the current estimates.

[57] Third, in situ sources of reactive nitrogen, lightning NO production and aircraft emissions, are examined. Lightning during the TRACE-P period was limited over India and Southeast Asia to latitudes lower than 30°N [*Fuelberg et al.*, 2003], and their contributions to the budget of reactive nitrogen in the present study area are therefore considered small. Influences from aircraft emissions are also considered to be small at altitudes below 7 km [e.g., *Koike et al.*, 2000]. Mixing of stratospheric air mass can increase ΔNO_y values, however results obtained using "Chinese air masses" (originated from below the 800-hPa level) are considered to have been influenced little.

[58] Fourth, transport of NO_y and SO_x in coarse mode particles is examined. As described in section 2, particulate matter with diameters greater than about 1 μm was not sampled either by aerosol composition measurement (PILS) or the NO_y measurement. Because of this size cut, the transport efficiencies estimated in this study are limited for gas phase and fine particles. It has been reported, however, that a significant amount of nitrate was contained in coarse mode aerosols sampled over the western Pacific [e.g., *Chen et al.*, 1997; *Kim and Park*, 2001]. If nitrate in these particles originated from anthropogenic NO_x emission, we have underestimated the total transport amount (gas + fine particles + coarse particles). Although coarse particles may not be very important for long-range transport due to their shorter residence time, they can play an important role in budget of reactive nitrogen. Three-dimensional model calculations for the East Asia region for March 1994 period also suggest that in the presence of mineral dust particles and sea-salt aerosols, a significant amount of HNO_3 is partitioned onto these particles because carbonate in the dust particles and chloride in sea-salt aerosols are volatile

and easily replaced by nitrate [*Song and Carmichael*, 2001]. During TRACE-P, coarse mode particles were also collected from the DC-8 [*Dibb et al.*, 2003]. Analyses using these aerosol data indicate that air masses with elevated levels of dust particles (high nssCa^{2+} levels) are generally mixed with pollutants because these air masses often passed over the northeastern part of China [*Jordan et al.*, 2003]. As a result of an efficient uptake of HNO_3 by the dust particles, particulate NO_3^- constituted 50% of the total NO_3^- (gas phase HNO_3 + particulate NO_3^-) on average in these air masses [*Jordan et al.*, 2003; *Dibb et al.*, 2003]. Because HNO_3 constitute 10–20% of NO_y (Figure 10a and Table 4), we could have underestimated the total transport efficiency of NO_y by 10–20%. Chemical conversion of SO_2 to sulfate on mineral dust particles may also take place [*Xiao et al.*, 1997]. Ground based measurements indicate that although most of the sulfate has been found on accumulation mode particles [*Chen et al.*, 1997], significant amounts were found in the coarse mode during heavy dust events [*Kim and Park*, 2001]. Though no major dust events occurred during TRACE-P, some signatures of uptake of SO_2 on dust particles were found from the DC-8 measurements [*Jordan et al.*, 2003]. More studies are needed in order for us to better understand the budget of nitrate and sulfate over East Asia.

[59] Finally, the approach using a single background value is examined, because it has been used in various studies [e.g., *Parrish et al.*, 1991; *Stohl et al.*, 2002; *Miyazaki et al.*, 2003]. When we use background values of CO and NO_y of 129 ppbv and 157 pptv, which are the minimum values at 0–2 km in the study area, a transport efficiency of NO_y for air masses used for the present study ($\Delta CO > 30$ ppbv in "continental air masses") at 0–2 km and 2–7 km is estimated to be 25–35% and 20%, respectively. This is well within the uncertainties in our estimate. Because the variability of the CO was large, the choice of a background CO level was not very critical during TRACE-P. However, if we use CO_2 as a reference, an error in the estimate will be large. This is because changes in CO_2 due to anthropogenic emissions were generally comparable to those caused by background air mass mixing.

6. Summary

[60] The transport efficiencies of NO_y and SO_x ($\varepsilon(NO_y)$ and $\varepsilon(SO_x)$) in the form of gas and fine particles (diameters smaller than 1 μm) were estimated for anthropogenic emissions from the northeastern part of China using NASA P-3B and DC-8 data obtained during the TRACE-P experiment, conducted over the western Pacific between February and April 2001. Transport efficiency was defined as the observed NO_y (SO_x) number density (over the background level) in one air mass divided by the expected increase in that air mass assuming that there is no loss after receiving anthropogenic emission (equations (1) and (2)). For this purpose, we introduced a new method to estimate the background levels of various species in individual air masses that have experienced multiple injection, mixing, and loss processes. In this method, a linear relationship between CO and CO_2 in background air masses was used instead of using a single value of CO or CO_2. When CO and CO_2 are higher than this background relationship, levels of Halon 1211 and OCS, which are considered to be unique tracers of emissions from China, are also higher, suggesting the validity of our approach. We then estimated an increase of CO, NO_y, and SO_x in individual air masses (ΔCO, ΔNO_y, and ΔSO_x), and the transport efficiencies were calculated using CO as a passive tracer.

[61] We selected the study area of 30°N–42°N and 124°E–140°E because air masses sampled in this area had mostly been transported from over the northeastern part of China and had little effects from a volcano on Miyakejima Island. Air masses sampled in the study area were denoted as "continental air masses" in this study. In addition, we defined "Chinese air masses" that passed over China at altitudes below the 800-hPa level (boundary layer) within 5 days prior to measurements without passing over South Korea or Japan at these low altitudes. "Chinese air" is a subset of "continental air." Emission inventory data showed a good correlation between emissions of CO, CO_2, NO_x, and SO_2 over the northeastern part of China (25°N–50°N and 100°E–130°E, except for South Korea region) where "continental air masses" had generally originated. This result indicates that various emission sources are generally co-located and ensure that the use of single emission ratios in our study, E_{CO}/E_{CO2}, E_{NOx}/E_{CO}, and E_{SO2}/E_{CO}, is reasonable.

[62] Averages of ΔCO, ΔNO_y, and ΔSO_x values were calculated for air masses in which $\Delta CO > 30$ ppbv in "continental air masses," and the transport efficiencies were calculated by taking their ratios. Vertical profiles of the transport efficiencies in "continental air masses" generally agreed with those in "Chinese air masses," within the uncertainties (50%). The results from the P-3B showed that 20–40% and 15% of NO_x emitted over the northeastern part of China remained as NO_y at 0–2 km (boundary layer) and 2–7 km (free troposphere), respectively. In the free troposphere, PAN was found to be the dominant form, while only 0.5% of emitted NO_x remained as NO_x. The transport efficiency of SO_x was estimated to be 25–45% and 15–20% in the boundary layer and free troposphere, respectively. Median values of SO_4^{2-}/SO_x ratio were 0.4–0.6 both in the boundary layer and free troposphere, though large variability was found in the free troposphere. These estimates were generally consistent with those derived using DC-8 data. The results obtained in this study indicate that more than half of NO_y and SO_x were lost over the continent and that the vertical transport from the boundary layer to the free troposphere further reduced their amounts by a factor of 2. Because HNO_3 + NO_3^- consisted of about 30–50% of NO_y at 0–2 km, a very efficient wet removal of these two compounds during the vertical transport was suggested to be responsible for the observed reduction in NO_y. Furthermore, a positive correlation between the transport efficiencies of NO_y and SO_x indicates that the loss processes of these two species likely proceeded simultaneously. In general, the transport efficiency has been estimated well, however relatively large uncertainties remain in the processes controlling the gas to particle conversion.

[63] The export flux fraction was also estimated for air masses which we sampled during TRACE-P. The export flux fraction was defined as the flux of observed NO_y (SO_x) molecules in each altitude range divided by the expected

total flux (surface to the tropopause) of NO_y (SO_x) molecules assuming that there is no loss after receiving anthropogenic emission (equation (4)). As a result, export flux fractions of NO_y at 0–2 km and 2–7 km were estimated to be 8% and 10%, respectively. The export flux fractions of SO_x in these two altitude ranges were estimated to be 10% and 12%, respectively. Flux in the boundary layer and free troposphere was found to have a similar contribution. This result is in contrast with that of CO in which flux in the free troposphere was greater. The difference was likely due to the wet removal of NO_y and SO_x during the vertical transport into the free troposphere.

[64] Budgets of NO_y and SO_x are estimated simply using the export flux fraction for air masses sampled during TRACE-P, although the measurements were quite limited in space and time. The estimates of the export flux fraction suggest that the total flux of NO_y and SO_x from the continent in these cases was 20% of the total emissions over the northeastern part of China.

[65] **Acknowledgments.** We are indebted to all of the TRACE-P participants for their cooperation and support. Special thanks are due to the flight and ground crews of the NASA P3-B and DC-8 aircraft for helping make this effort a success. We thank N. Toriyama, M. Kanada, and H. Jindo at Solar-Terrestrial Environment Laboratory, Nagoya University, Japan, for their technical assistance with the measurements of NO, NO_2, and NO_y. We also thank B. Liley at National Institute of Water and Atmospheric Research Ltd. (NIWA), New Zealand for calculating the cutoff size for NO_y measurements by numerical simulations. The meteorological data were supplied by the European Center for Medium-Range Weather Forecasts (ECMWF). This work was supported in part by the Ministry of Education, Culture, Sports, Science, and Technology (MEXT). The trajectory calculation program used in this paper was developed by Y. Tomikawa and K. Sato at National Institute of Polar Research, Japan.

References

Bey, I., D. J. Jacob, J. A. Logan, and R. M. Yantosca, Asian chemical outflow to the Pacific in spring: Origins, pathways, and budgets, *J. Geophys. Res.*, *106*, 23,097–23,113, 2001.

Blake, N. J., et al., Large-scale latitudinal and vertical distribution of NMHCs and selected halocarbons in the troposphere over the Pacific Ocean during the March–April 1999 Pacific Exploratory Mission (PEM-Tropics B), *J. Geophys. Res.*, *106*, 32,627–32,644, 2001.

Blake, N. J., et al., NMHCs and halocarbons in Asian continental outflow during TRACE-P: Comparison to PEM-West B, *J. Geophys. Res.*, *108*(D20), 8806, doi:10.1029/2002JD003367, in press, 2003.

Bradshaw, J., et al., Photofragmentation two-photon laser-induced fluorescence detection of NO_2 and NO: Comparison of measurements with model results based on airborne observations during PEM-Tropics A, *Geophys. Res. Lett.*, *26*, 471–474, 1999.

Carmichael, G. R., et al., Aerosol composition at Cheju Island, Korea, *J. Geophys. Res.*, *102*, 6047–6061, 1997.

Carmichael, G. R., et al., Evaluating regional emission estimates using the TRACE-P observations, *J. Geophys. Res.*, *108*(D21), 8810, doi:10.1029/2002JD003116, in press, 2003.

Chen, L.-L., et al., Influence of continental outflow events on the aerosol composition at Cheju Island, South Korea, *J. Geophys. Res.*, *102*, 28,551–28,574, 1997.

Chin, M., and D. D. Davis, A reanalysis of carbonyl sulfide as a source of stratospheric background sulfur aerosol, *J. Geophys. Res.*, *100*, 8993–9005, 1995.

Chin, M., et al., Atmospheric sulfur cycle simulated in the global model GOCART: Comparison with field observations and regional budgets, *J. Geophys. Res.*, *105*, 24,689–24,712, 2000.

Dibb, J. E., R. W. Talbot, E. Scheuer, G. Seid, M. Avery, and H. Singh, Aerosol chemical composition in Asian continental outflow during TRACE-P: Comparison to PEM-West B, *J. Geophys. Res.*, *108*(D21), 8815, doi:10.1029/2002JD003111, in press, 2003.

Eisele, F., et al., Summary of measurement intercomparisons during TRACE-P, *J. Geophys. Res.*, *108*(D20), 8791, doi:10.1029/2002JD003167, in press, 2003.

Fraser, P. J., D. E. Oram, C. E. Reeves, S. A. Penkett, and A. McCulloch, Southern hemispheric halon trends (1978–1998) and global halon emissions, *J. Geophys. Res.*, *104*, 15,985–15,999, 1999.

Fuelberg, H. E., C. M. Kiley, J. R. Hannan, D. J. Westberg, M. A. Avery, and R. E. Newwell, Meteorological conditions and transport pathways during the Transport and Chemical Evolution over the Pacific (TRACE-P) experiment, *J. Geophys. Res.*, *108*(D20), 8782, doi:10.1029/2002JD003092, in press, 2003.

Hao, J., H. Tian, and Y. Lu, Emission inventories of NO_x from commercial energy consumption in China, 1995–1998, *Environ. Sci. Technol.*, *36*, 552–560, 2002.

Heald, C. L., D. J. Jacob, P. I. Palmer, M. J. Evans, G. W. Sachse, H. B. Singh, and D. R. Blake, Biomass burning emission inventory with daily resolution: Application to aircraft observations of Asian outflow, *J. Geophys. Res.*, *108*(D21), 8811, doi:10.1029/2002JD003082, in press, 2003.

Jacob, D. J., et al., The transport and chemical evolution over the Pacific (TRACE-P) mission: Design, execution, and overview of results, *J. Geophys. Res.*, *108*(D20), 8781, doi:10.1029/2002JD003276, in press, 2003.

Jaffe, D., et al., Transport of Asian air pollution to North America, *Geophys. Res. Lett.*, *26*, 711–714, 1999.

Jordan, C. E., J. E. Dibb, B. E. Anderson, and H. E. Fuelberg, Uptake of nitrate and sulfate on dust aerosols during TRACE-P, *J. Geophys. Res.*, *108*(D21), 8817, doi:10.1029/2002JD003101, in press, 2003.

Kim, B., and S. Park, Transport and evolution of a winter-time Yellow sand observed in Korea, *Atmos. Environ.*, *35*, 3191–3201, 2001.

Kim, B., J. Han, and S. Park, Transport of SO_2 and aerosol over the Yellow Sea, *Atmos. Environ.*, *35*, 727–737, 2001.

Koike, M., Y. Kondo, S. Kawakami, H. Nakajima, G. L. Gregory, G. W. Sachse, H. B. Singh, E. V. Browell, J. T. Merrill, and R. E. Newell, Reactive nitrogen and its correlation with O_3 and CO over the Pacific in winter and early spring, *J. Geophys. Res.*, *102*, 28,385–28,404, 1997.

Koike, M., et al., Impact of aircraft emissions on reactive nitrogen over the North Atlantic Flight Corridor region, *J. Geophys. Res.*, *105*, 3665–3677, 2000.

Koike, M., et al., Redistribution of reactive nitrogen in the Arctic lower stratosphere in the 1999–2000 winter, *J. Geophys. Res.*, *107*(D20), 8275, doi:10.1029/2001JD001089, 2002.

Kondo, Y., S. Kawakami, M. Koike, D. W. Fahey, H. Nakajima, N. Toriyama, M. Kanada, Y. Zhao, G. W. Sachse, and G. L. Gregory, The performance of an aircraft instrument for the measurement of NOy, *J. Geophys. Res.*, *102*, 28,663–28,671, 1997.

Liu, H., D. J. Jacob, I. Bey, R. M. Yantosca, B. N. Duncan, and G. W. Sachse, Transport pathways for Asian combustion outflow over the Pacific: Interannual and seasonal variations, *J. Geophys. Res.*, *108*(D20), 8786, doi:10.1029/2002JD003102, in press, 2003.

Ma, Y., et al., Intercomparison of airborne measurements of aerosol ionic chemical composition during TRACE-P and ACE-Asia, *J. Geophys. Res.*, *108*(D21), 8816, doi:10.1029/2002JD003128, in press, 2003.

Mari, C., D. J. Jacob, and P. Bechtold, Transport and scavenging of soluble gases in a deep convective cloud, *J. Geophys. Res.*, *105*, 22,255–22,267, 2000.

Mauldin, R. L., III, D. J. Tanner, and F. L. Eisele, A new chemical ionization mass spectrometer technique for the fast measurement of gas phase nitric acid in the atmosphere, *J. Geophys. Res.*, *103*, 3361–3367, 1998.

Miyazaki, Y., et al., Synoptic-scale transport of reactive nitrogen over the western Pacific in spring, *J. Geophys. Res.*, *108*(D20), 8788, doi:10.1029/2002JD003248, in press, 2003.

Moxim, W. J., H. Levy II, and P. S. Kasibhatla, Simulated global tropospheric PAN: Its transport and impact on NO_x, *J. Geophys. Res.*, *101*, 12,821–12,638, 1996.

Palmer, P. I., et al., Top-down emission inventory of carbon monoxide from Asia using aircraft observations from TRACE-P, *J. Geophys. Res.*, *108*(D21), 8828, doi:10.1029/2003JD003397, in press, 2003.

Parrish, D. D., M. Trainer, M. P. Buhr, B. A. Watkins, and F. C. Fehsenfeld, Carbon monoxide concentrations and their relation to concentrations of total reactive oxidized nitrogen at two rural U.S. sites, *J. Geophys. Res.*, *96*, 9309–9320, 1991.

Sachse, G. W., G. F. Hill, L. O. Wade, and M. G. Perry, Fast-response, high-precision carbon monoxide sensor using a tunable diode laser absorption technique, *J. Geophys. Res.*, *92*, 2071–2081, 1987.

Scheuer, E., R. Talbot, J. Dibb, G. Seid, and B. Lefer, Seasonal distributions of fine aerosol sulfate in the North American Arctic basin during TOPSE, *J. Geophys. Res.*, in press, 2002.

Singh, H. B., et al., Reactive nitrogen and ozone over the western Pacific: Distribution, partitioning, and sources, *J. Geophys. Res.*, *101*, 1793–1808, 1996.

Song, C. H., and G. R. Carmichael, Gas-particle partitioning of nitric acid modulated by alkaline aerosol, *J. Atmos. Chem.*, *40*, 1–22, 2001.

Stohl, A., M. Trainer, T. B. Ryerson, J. S. Holloway, and D. D. Parrish, Export of NO_y from the North American boundary layer during 1996 and 1997 North Atlantic Regional Experiments, *J. Geophys. Res.*, *107*(D11), 4131, doi:10.1029/2001JD000519, 2002.

Streets, D. G., N. Y. Tsai, H. Akimoto, and K. Oka, Sulfur dioxide emissions in Asia in the period 1985–1997, *Atmos. Environ.*, *34*, 4413–4424, 2000.

Streets, D. G., et al., An inventory of gaseous and primary aerosol emissions in Asia in the year 2000, *J. Geophys. Res.*, *108*(D21), 8809, doi:10.1029/2002JD003093, in press, 2003.

Talbot, R. W., et al., Large-scale distributions of tropospheric nitric, formic, and acetic acids over the western Pacific basin during wintertime, *J. Geophys. Res.*, *102*, 28,303–28,313, 1997.

Tan, Q., Y. Huang, and W. L. Chameides, Budget and export of anthropogenic SO_x from East Asia during continental outflow condition, *J. Geophys. Res.*, *107*(D13), 4167, doi:10.1029/2001JD000769, 2002.

Thornton, D. C., A. R. Bandy, F. H. Tu, B. W. Blomquist, G. M. Mitchell, W. Nadler, and D. Lenschow, Fast airborne sulfur dioxide measurements by atmospheric pressure ionization mass spectrometry (APIMS), *J. Geophys. Res.*, *107*(D22), 4632, doi:10.1029/2002JD002289, 2002.

van Aardenne, J. A., G. R. Carmichael, H. Levy II, D. Streets, and L. Hordijk, Anthropogenic NO_x emissions in Asia in the period 1990–2020, *Atmos. Environ.*, *33*, 633–646, 1999.

Vay, S. A., B. E. Anderson, T. J. Conway, G. W. Sachse, J. E. Collins Jr., D. R. Blake, and D. J. Westberg, Airborne observations of the tropospheric CO_2 distribution and its controlling factors over the South Pacific Basin, *J. Geophys. Res.*, *104*, 5663–5676, 1999.

Vay, S. A., et al., The influence of regional-scale anthropogenic emissions on CO_2 distributions over the western North Pacific, *J. Geophys. Res.*, *108*(D20), 8801, doi:10.1029/2002JD003094, in press, 2003.

Weber, R. J., D. Orsini, Y. Daun, Y.-N. Lee, P. J. Klotz, and F. Brechtel, A particle-into-liquid collector for rapid measurement of aerosol bulk chemical composition, *J. Aerosol Sci. Technol.*, *35*, 718–727, 2001.

Xiao, H., G. R. Carmichael, J. Durchenwald, D. Thornton, and A. Bandy, Long-range transport of SO_x and dust in East Asia during the PEM B experiment, *J. Geophys. Res.*, *102*, 28,589–28,612, 1997.

D. R. Blake, Department of Chemistry, University of California, Irvine, Irvine, CA 92697-2025, USA. (dblake@orion.oac.uci.edu)

F. L. Eisele, F. Flocke, and A. J. Weinheimer, Atmospheric Chemistry Division, National Center for Atmospheric Research, Boulder, CO 80303, USA. (eisele@ncar.ucar.edu; ffl@acd.ucar.edu; wein@ucar.edu)

K. Kita, Department of Environmental Sciences, Faculty of Science, Ibaraki University, 2-1-1 Bunkyo, Mito, Ibaraki 310-8512, Japan. (kita@env.sci.ibaraki.ac.jp)

M. W. Ko, G. W. Sachse, and S. A. Vay, Langley Research Center, Mail Stop 401B, 21 Langley Boulevard, Hampton, VA 23681-2199, USA. (m.k.ko@larc.nasa.gov; g.w.sachse@larc.nasa.gov; s.a.vay@larc.nasa.gov)

M. Koike and Y. Masui, Department of Earth and Planetary Science, Graduate School of Science, The University of Tokyo, Hongo 7-3-1, Bunkyo-ku, Tokyo, 113-0033, Japan. (koike@eps.s.u-tokyo.ac.jp; masui@aos.eps.s.u-tokyo.ac.jp)

Y. Kondo, Y. Miyazaki, and N. Takegawa, Research Center for Advanced Science and Technology, University of Tokyo, 4-6-1 Komaba, Meguro, Tokyo 153-8904, Japan. (kondo@atmos.rcast.u-tokyo.ac.jp; yuzom@atmos.rcast.u-tokyo.ac.jp; takegawa@atmos.rcast.u-tokyo.ac.jp)

S. T. Sandholm and R. J. Weber, Department of Earth and Atmospheric Sciences, Georgia Institute of Technology, Atlanta, GA 30332, USA. (scott.sandholm@eas.gatech.edu; rweber@eas.gatech.edu)

H. B. Singh, NASA Ames Research Center, Moffett Field, CA 94035, USA. (hsingh@mail.arc.nasa.gov)

D. G. Streets, Decision and Information Sciences Division, Argonne National Laboratory, Argonne, IL 60439-4803, USA. (dstreets@anl.gov)

R. W. Talbot, University of New Hampshire, Durham, NH 03820, USA. (robert.talbot@unh.edu)

D. C. Thornton, Department of Chemistry, Drexel University, Philadelphia, PA 19104, USA. (dct@drexel.edu)